Neuron

Article

Stress relief as a natural resilience mechanism against depression-like behaviors

Graphical abstract

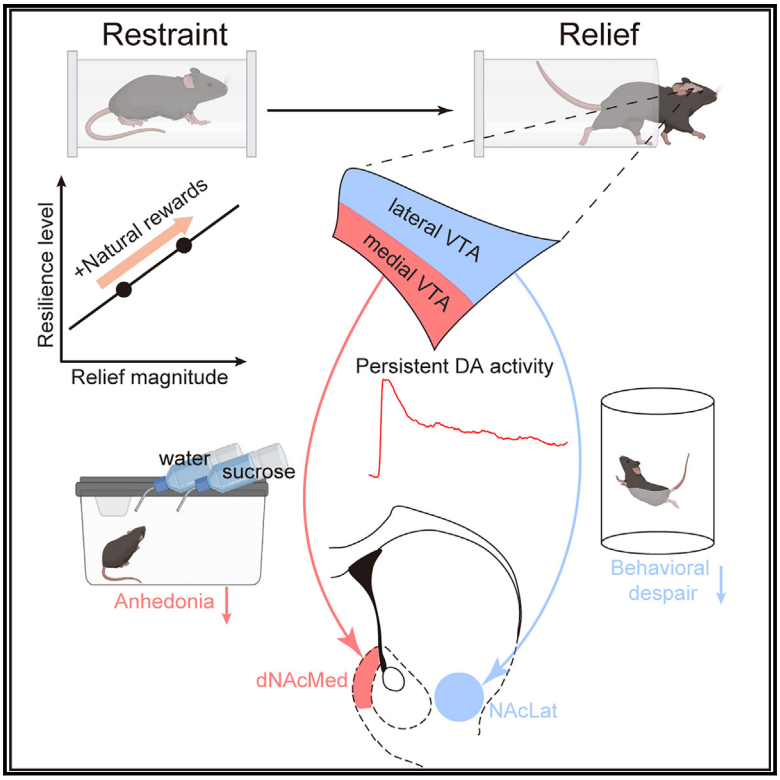

Authors

Yiyan Dong, Yifei Li, Xinkuan Xiang, ..., Yulong Li, Haohong Li, Hailan Hu

Correspondence

huhailan@zju.edu.cn

In brief

Dong et al. identify stress relief as a natural resilience mechanism against depression-like behaviors, delineate underlying dissociable mesoaccumbal dopamine circuits for preventing despair or anhedonia, and introduce a non-invasive behavioral strategy for promoting resilience.

Highlights

- Magnitude of stress relief positively correlates with resilience to depression
- Stress relief persistently activates VTA-DA neurons
- DA projections to NAcLat and dNAcMed encode relief to prevent despair and anhedonia
- Providing natural rewards at stress termination increases resilience to depression

Dong et al., 2023, Neuron *111*, 1–13
December 6, 2023
https://doi.org/10.1016/j.neuron.2023.09.004

CellPress

Neuron

CellPress

Article

Stress relief as a natural resilience mechanism against depression-like behaviors

Yiyan Dong,[1,2] Yifei Li,[2] Xinkuan Xiang,[2] Zhuo-Cheng Xiao,[3] Ji Hu,[4] Yulong Li,[5] Haohong Li,[2] and Hailan Hu[1,2,6,*]

[1]Department of Psychiatry and International Institutes of Medicine, The Fourth Affiliated Hospital, Zhejiang University School of Medicine, Yiwu 322000, China

[2]Liangzhu Laboratory, MOE Frontier Science Center for Brain Science and Brain-Machine Integration, State Key Laboratory of Brain-Machine Intelligence, New Cornerstone Science Laboratory, Zhejiang University, Hangzhou 311121, China

[3]Courant Institute of Mathematical Sciences, New York University, New York, NY 10003, USA

[4]School of Life Science and Technology, ShanghaiTech University, Shanghai 201210, China

[5]State Key Laboratory of Membrane Biology, Peking University School of Life Sciences, Beijing 100871, China

[6]Lead contact

*Correspondence: huhailan@zju.edu.cn

https://doi.org/10.1016/j.neuron.2023.09.004

SUMMARY

Relief, the appetitive state after the termination of aversive stimuli, is evolutionarily conserved. Understanding the behavioral role of this well-conserved phenomenon and its underlying neurobiological mechanisms are open and important questions. Here, we discover that the magnitude of relief from physical stress strongly correlates with individual resilience to depression-like behaviors in chronic stressed mice. Notably, blocking stress relief causes vulnerability to depression-like behaviors, whereas natural rewards supplied shortly after stress promotes resilience. Stress relief is mediated by reward-related mesolimbic dopamine neurons, which show minute-long, persistent activation after stress termination. Circuitry-wise, activation or inhibition of circuits downstream of the ventral tegmental area during the transient relief period bi-directionally regulates depression resilience. These results reveal an evolutionary function of stress relief in depression resilience and identify the neural substrate mediating this effect. Importantly, our data suggest a behavioral strategy of augmenting positive valence of stress relief with natural rewards to prevent depression.

INTRODUCTION

One fascinating feature of emotions is that positive and negative states can be intertwined and interact intimately.[1–5] In particular, mysteriously, the ending of a strong emotional state is often followed by a state of opposite valence.[6] Although the aversive withdrawal state from the substance-induced euphoric mood has been extensively investigated,[7–11] the opposite phenomenon, that is, the appetitive state after the termination of negative stimuli—the so-called "relief"—is much less explored.

The positive valence of relief has been demonstrated in flies, rodents, and humans.[6,12–14] Utilizing the appetitive state of relief, researchers have built relief learning paradigms, associating cues with the ending/omission of stress, threat, or pain, to reinforce behaviors.[15–18] Pharmacology and recent neural circuit studies suggest that the dopamine (DA) system is activated and required for relief-based learnings.[19–24] However, despite progress in relief learning, several fundamental questions have remained unanswered about stress relief per se: how do DA neurons and their downstream projections encode stress relief, and, in what timescale? What is the evolutionary purpose of having a state of relief? And can this positive emotional state be harnessed to combat psychiatric disorders such as depression?

Stress is known to trigger depression in some individuals but resilience in others.[25,26] The neurobiological basis for such individual differences in stress resilience has been demonstrated as a series of active coping processes.[27,28] Recent studies reveal resilience mechanisms at multiple levels, involving epigenetic modulation, neuronal activity, and neurogenesis.[29–33] At the neural circuit level, a causal role of the ventral tegmental area (VTA) DA circuitry in modulating resilience is highlighted.[34–38] The inherent opponency in the valence between stress and relief raises the intriguing possibility that relief may counteract the detrimental effects of stress, playing a role in stress resilience. However, such a possibility has not been tested experimentally.

To address these questions, we employed calcium photometry as well as electrophysiological and optogenetic techniques to explore the function of stress relief in depression resilience. We provided scalable measurement of stress relief in mice and identified its appetitive valence and transient time window. Notably, we found that the magnitude of stress relief positively correlated with the resilience level to depression-like behaviors

Please cite this article in press as: Dong et al., Stress relief as a natural resilience mechanism against depression-like behaviors, Neuron (2023), https://doi.org/10.1016/j.neuron.2023.09.004

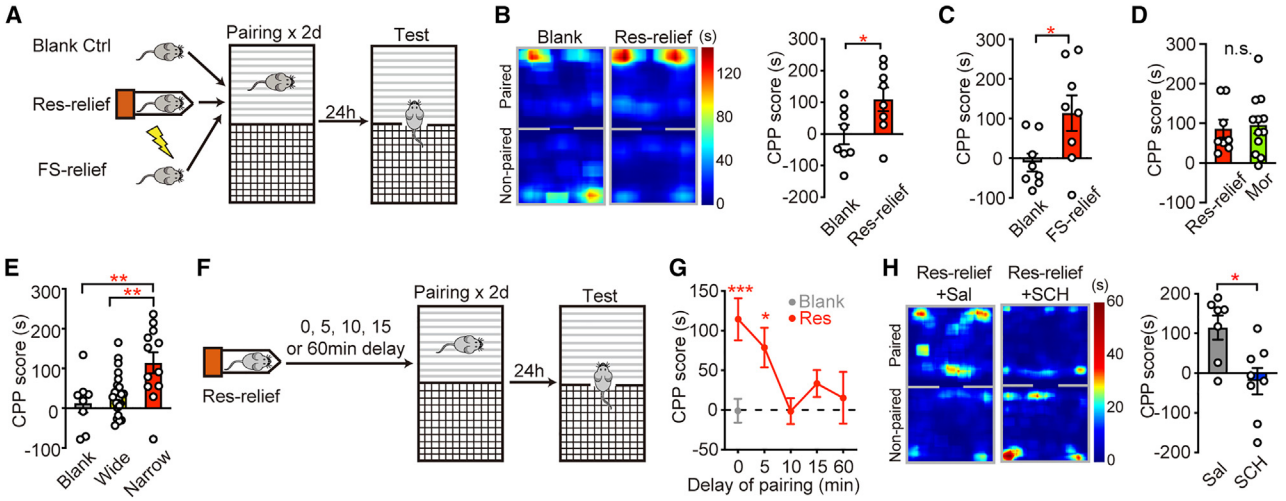

Figure 1. Stress relief evokes a transient strong reward effect, which requires the DA system

(A) Behavioral schematics of blank control, restraint (Res)-relief, or foot shock (FS)-relief-paired conditioned place preference (CPP).

(B) CPP test heatmaps of example mice paired with blank or Res-relief (left) and quantification of CPP score (right).

(C) Quantification of FS-relief CPP score.

(D) CPP score induced by Res-relief or morphine.

(E) Relief CPP score from restraint stress using different diameters of tubes.

(F) Behavioral schematics of Res-relief CPP with different time delay before relief pairing.

(G) Quantification of time window of Res-relief CPP.

(H) CPP test heatmaps of example mice paired with Res-relief and i.p. injection of saline or D1R antagonist SCH23390 (left), and quantification of CPP score (right).

n.s., not significant; *p < 0.05, **p < 0.01, ***p < 0.001; data represent mean ± SEM.

See also Table S1.

in chronic stressed mice. Fiber photometry and *in vivo* optogenetic manipulations demonstrated that stress relief recruited separate mesoaccumbal DA projections to the nucleus accumbens lateral shell (NAcLat) and dorsomedial shell (dNAcMed) to prevent distinct aspects of depression-like phenotypes. By blocking or enhancing stress relief, we were able to either promote or prevent depression-like behaviors. Collectively, our data suggest that stress relief serves as a natural resilience mechanism against depression, proposing a non-invasive behavioral strategy to increase resilience.

RESULTS

Stress relief evokes strong and transient rewarding effects

To assess the valence of emotion at the termination of aversive events, we subjected male C57BL/6 mice to the conditioned place preference (CPP) test.[39,40] Immediately after a restraint session, we placed mice in one of the two chambers for 30 min, repeated this procedure once per day for 2 days, and 24 h after the final pairing session, tested for their CPP score (restraint [Res]-relief CPP, see STAR Methods; Figure 1A). Compared with the blank-paired control, mice displayed robust preference for the Res-relief-paired chamber (Figure 1B), suggesting that relief from restraint stress evokes a positive conditioning valence state. To further explore whether the rewarding effect of stress relief is common to different aversive stimuli, we applied another stressor—one which recruits different sensory modalities—unexpected foot shock (0.5 mA, 2-s duration, 10 stimuli; foot shock [FS]-relief CPP, Figure 1A). Mice also displayed strong place preference for the FS-relief-paired chamber (Figure 1C). Notably, the magnitude of rewarding effect from stress relief as measured by CPP level is as large as that caused by morphine, a potently hedonic agent (Figure 1D). Restraint in a wider tube (see STAR Methods) caused no CPP effect (Figure 1E), indicating that the rewarding effect of stress relief depends on the aversiveness of the stressor.

To map the time window of the stress relief effect, we introduced different time delays between the restraint ending and introduction to the pairing chamber (Figure 1F). Within 10 min of the termination of restraint, the rewarding effect rapidly diminished (Figure 1G), indicating that the appetitive effect of stress relief is transient. Next, to see whether extending the restraint period would extend the duration of relief, we prolonged the restraint period from 30 min to 2 h. The appetitive relief state remained transient and still diminished within 10 min (Figure S1A). In addition, intraperitoneal (i.p.) injection of selective DA D1 receptor (D1R) antagonist SCH23390 (SCH) led to diminished relief after the CPP (Figure 1H), suggesting that stress relief requires a D1R-dependent DA signaling mechanism.

Magnitude of stress relief positively correlates with level of resilience to depression-like behaviors

To test a potential function of relief in stress resilience, we first examined the correlation between the magnitude of stress relief and the severity of depression-like behaviors after chronic stress

Please cite this article in press as: Dong et al., Stress relief as a natural resilience mechanism against depression-like behaviors, Neuron (2023), https://doi.org/10.1016/j.neuron.2023.09.004

CellPress

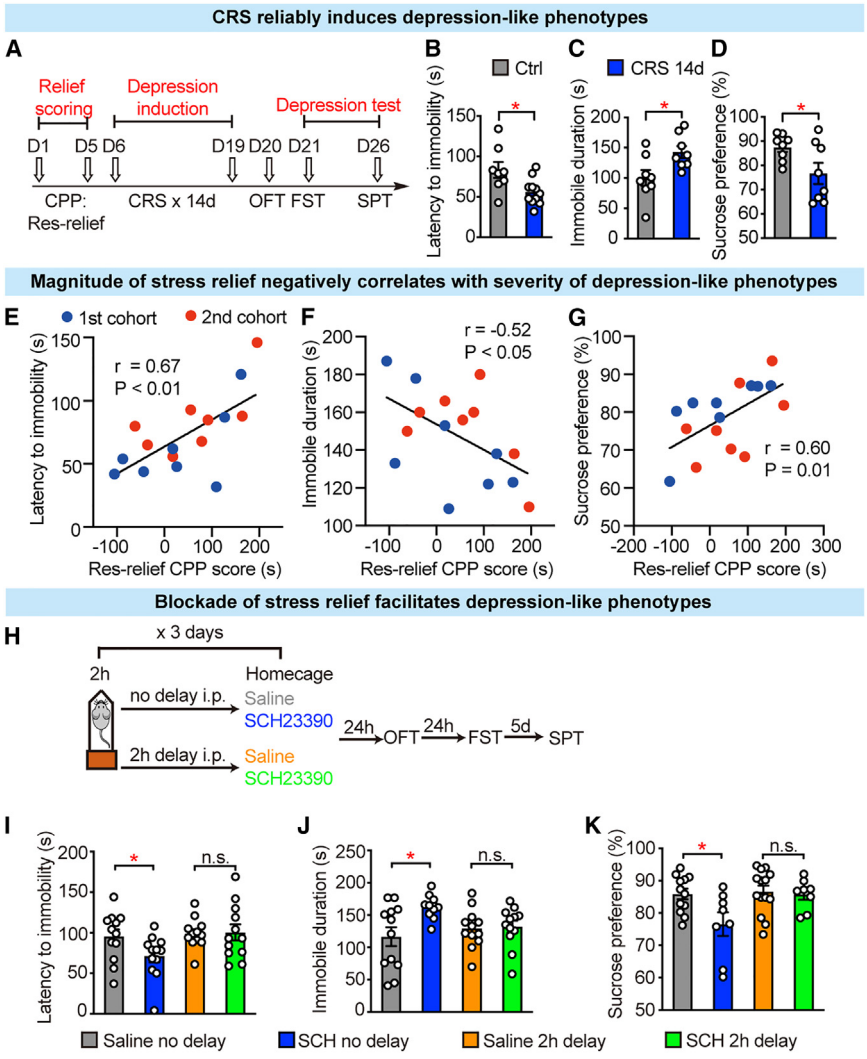

Figure 2. Stress relief is correlated with and required for resilience to depression-like behaviors

(A) Behavioral timeline of Res-relief CPP scoring, CRS induction, and depression-like phenotype measurement.

(B–D) Depression-like phenotypes induced by 14-day CRS: latency to immobility (B) and immobile duration (C) in FST, and sucrose preference (D) in SPT.

(E–G) Correlation analysis between Res-relief CPP score and latency to immobility (E), immobile duration (F), and sucrose preference (G) of CRS mice.

(H–K) Behavioral paradigm of systemic D1R blockade, with or without 2-h delay after terminating daily restraint during subthreshold 3-day CRS (H), and subsequent depression-like phenotypes developed in FST (I and J) and SPT (K).

n.s., not significant; *p < 0.05; data represent mean ± SEM.

See also Figures S1–S3 and Table S1.

across mouse individuals. Mice were first tested in the Res-relief CPP paradigm and then subjected to a chronic restraint stress (CRS) protocol (2-week consecutive restraint stress, 2–3 h per day)[41,42] to induce depression-like behaviors (Figure 2A). After CRS, a large fraction of mice developed depression-like behaviors, including behavioral despair measured by the forced swim test (FST) (Figures 2B and 2C), and anhedonia-like phenotypes measured by the sucrose preference test (SPT) (Figure 2D), without affecting locomotion and anxiety in the open field test (OFT) (Figures S1B and S1C). Notably, the magnitude of stress relief as measured by the CPP score after restraint stress (Res-relief CPP score) showed a significant negative correlation with the severity of depression-like behaviors: animals with higher relief CPP score showed longer latency to immobility ($p < 0.01$, $r = 0.67$, Pearson correlation, Figure 2E) and shorter immobile duration ($p < 0.05$, $r = -0.52$, Pearson correlation, Figure 2F) in the FST, as well as higher sucrose preference in the SPT ($p = 0.01$, $r = 0.60$, Pearson correlation, Figure 2G). In contrast, the Res-relief CPP score did not correlate with locomotion ability as measured by OFT (Figure S2A), or anxiety level as measured by elevated plus maze test (EPMT) (Figure S2B), novelty-suppressed feeding test (NSFT) (Figure S2C), and OFT (Figure S2D). These results suggest that the more rewarding the animals feel at stress termination, the more resilient they are to depression-like behaviors.

Blockade of stress relief promotes vulnerability to depression-like behaviors

To test whether stress relief is indeed protective for depression-like behaviors, we blocked stress relief during the CRS procedure. We applied a subthreshold CRS protocol (3-day restraint stress, 2–3 h per day, Figure 2H), which normally did not induce depression-like phenotypes (Figures S3A–S3C). However, when stress relief was blocked by injection of the D1R antagonist SCH (i.p., 0.1 mg/kg) right after the termination of daily restraint, mice developed depression-like phenotypes after the subthreshold CRS. Compared with the saline-injected group, SCH-injected mice were more immobile in the FST (Figures 2I and 2J) and had less preference for sucrose water in the SPT (Figure 2K), with no apparent difference in locomotion (Figure S1D) or anxiety level (Figure S1E). As stress relief appeared to be transient, we therefore included another two control groups, with SCH injected either 2 h or 10 min after the termination of daily restraint (Figures 2H and S3F). No depression-like phenotypes were induced in these mice (Figures 2I–2K and S3G–S3I). These results suggest that blockade of stress relief within its transient time window makes animals more vulnerable to depression-like behaviors.

Stress relief persistently activates VTA-DA neurons

To understand the neural circuit mechanism mediating stress relief, we next set out to test whether and how the VTA-DA

Please cite this article in press as: Dong et al., Stress relief as a natural resilience mechanism against depression-like behaviors, Neuron (2023), https://doi.org/10.1016/j.neuron.2023.09.004

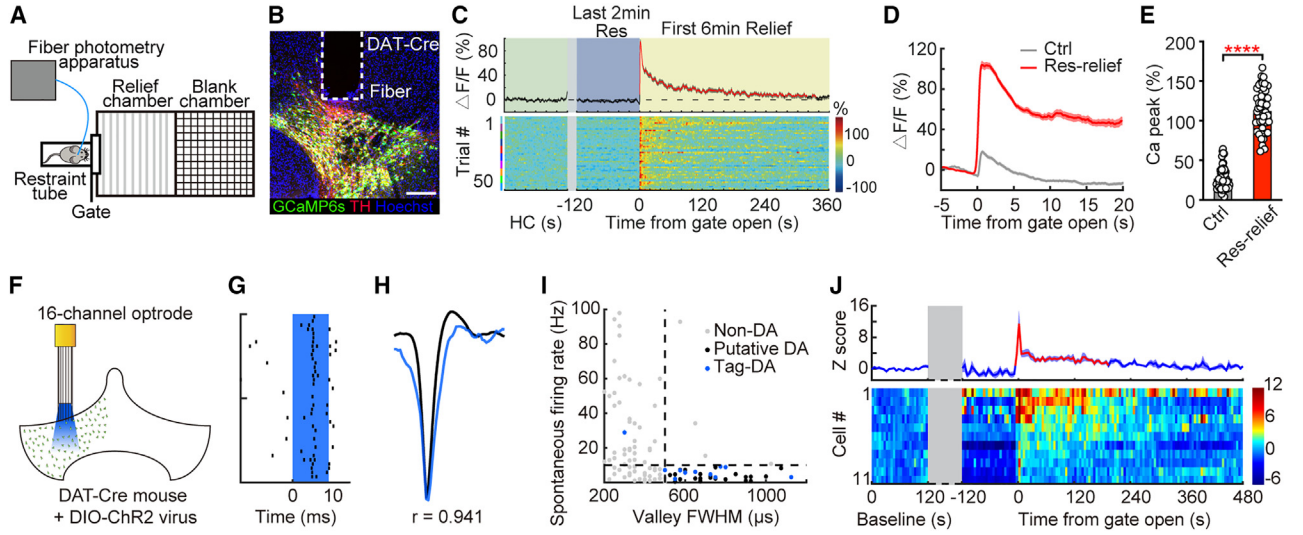

Figure 3. Stress relief persistently activates VTA-DA neurons

(A) Schematics of fiber photometry setup and Res-relief box to minimize human handling.

(B) Verifications of optic fiber location and Cre-dependent GCaMP6s expression profile in VTA-DA neurons. Scale bars, 200 μm.

(C) Calcium signals of VTA-DA soma aligned to the time point of gate open (top) and corresponding heatmaps (bottom, mouse individuals are annotated by different color bars at the left).

(D) Calcium signals of VTA-DA soma of Res-relief and control groups.

(E) Quantification of calcium peak amplitude of VTA-DA soma.

(F) Schematics of *in vivo* opto-tagged recording of VTA-DA neurons.

(G) Raster plot of one representative tagged DA neuron responding to light stimulation.

(H) Correlation between light-evoked and spontaneous spike waveforms of a representative tagged DA neuron.

(I) Classification of recorded VTA neurons based on full-width half maximum (FWHM) of waveform valley and spontaneous firing rate.

(J) Firing *Z* score of VTA-DA neurons aligned to the time point of gate open (top) and corresponding heatmaps (bottom), ordered by the activation magnitude during relief period.

Calcium signals or firing *Z* score significantly higher than baseline is annotated in red.

****$p < 0.0001$; data represent mean ± SEM.

See also Figures S4, S5, and S7, and Table S1.

neurons are activated during the relief period. To minimize the artifacts caused by human handling, we modified the CPP apparatus and connected it to the restraint tube through a gate, such that at the end of restraint stress, when the gate was opened, the mouse could voluntarily enter the relief chamber without human handlings (see STAR Methods; Figure 3A). Cre-dependent GCaMP6s was injected into the VTA of DAT-Cre mice and an optic fiber was implanted above the injection site (Figure 3B). The populational calcium response of VTA-DA somata was recorded before, during, and after the 30-min restraint (Figure 3C). The VTA-DA calcium signals showed a drastic increase when mice started to leave the restraint tube (peak △F/F = 94.83% ± 4.15%, $p < 0.0001$, permutation test, Figure 3C). The increase of VTA-DA calcium signals peaked at 0.6 ± 0.04 s and remained statistically higher than the homecage baseline for 317.8 s (~5.3 min, Figure 3C, permutation test). Because VTA-DA neurons can also be activated by saliency, novelty, or movement,[43,44] we also included a control condition to minimize the relief signals, by subjecting mice to immediate gate open after being placed in the restraint tube (see STAR Methods). The VTA-DA calcium peak amplitude of this control condition was much smaller than that of the stress-relief condition (△F/F = 27.4% ± 1.8% vs. 112.7% ± 3.7%, $p < 0.0001$, Figures 3D and 3E).

The above results indicate that the bulk activity of VTA-DA neurons is persistently increased during stress relief. However, it remained unclear whether such persistent activity holds at the single-neuron level. For instance, different populations of DA neurons may be activated at different time points after stress termination, resulting in a prolonged bulk activity. To address this issue, we performed opto-tagged *in vivo* recordings of VTA-DA neurons in freely moving mice (Figure 3F). Among 79 well-isolated neurons, based on opto-tagging criteria,[45,46] we reliably identified 11 DA neurons (Figures 3G–3I). Among these, 55% (6 out of 11) exhibited minute-level sustained activation during the relief period (*Z* score > 2, see STAR Methods; Figure 3J, bottom). The average activity of the 11 DA neurons remained above the baseline for 3 min (Figure 3J, top). In order to increase the number of DA neurons to substantiate our speculation, we classified putative DA neurons via spontaneous firing rate (<10 Hz) and valley full-width half maximum (FWHM, >500 μs), which has been validated via opto-tagging.[46] Among the 38 putative DA neurons identified (Figure S4A), 63% (24 out of 38) exhibited minute-level sustained activation (*Z* score > 2) and their average activity persisted for 150 s after stress termination (Figure S4B).

Please cite this article in press as: Dong et al., Stress relief as a natural resilience mechanism against depression-like behaviors, Neuron (2023), https://doi.org/10.1016/j.neuron.2023.09.004

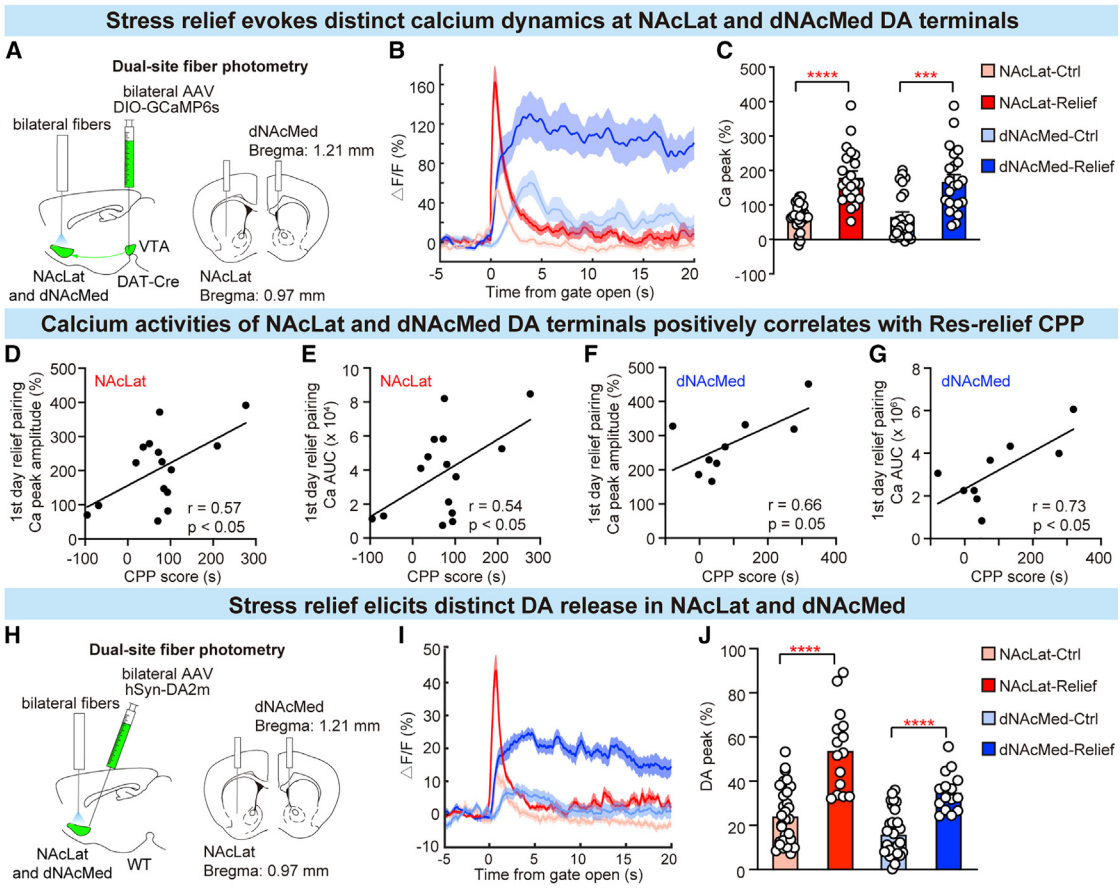

Figure 4. Activities of VTA-NAcLat and -dNAcMed DA pathways correlate with magnitude of stress relief

(A) Schematics of simultaneous dual-site fiber photometry of DA terminal calcium signals in NAcLat and dNAcMed.

(B) Calcium signals of NAcLat and dNAcMed DA terminals in Res-relief and control groups.

(C) Quantification of calcium peak amplitude of NAcLat and dNAcMed DA terminals.

(D–G) Correlation of Res-relief CPP score with NAc DA terminal calcium signals during the 1st day of relief pairing: calcium peak amplitude (D), area under curve (AUC) (E) of NAcLat DA terminals; calcium peak amplitude (F) and AUC (G) of dNAcMed DA terminals. These results are acquired by single-site fiber photometry.

(H) Schematics of simultaneous dual-site fiber photometry of DA release in NAcLat and dNAcMed.

(I) DA signals in NAcLat and dNAcMed of Res-relief and control groups.

(J) Quantification of DA peak amplitude in NAcLat and dNAcMed.

***p < 0.001, ****p < 0.0001; data represent mean ± SEM.

See also Figures S4, S6, and S7 and Table S1.

These results suggest that the prolonged VTA-DA activity is not due to desynchronized activation in the populational level but rather due to sustained activation at the single-cell level.

Distinct activity dynamics of DA projections to different NAc subregions during stress relief

Previous studies revealed that VTA-DA neurons are functionally heterogeneous in encoding reward and aversion[47–53] and that such heterogeneity may be defined by distinct downstream projections.[54–58] Among the VTA-DA projections, while the amygdala- and prefrontal-projecting DA pathways encode salience and aversion,[59–64] the mesoaccumbal DA pathways have been heavily implicated in reward processing,[60,65–69] particularly the DA projections to the NAcLat and dNAcMed.[23,61,70,71] Therefore, we applied dual-site fiber photometry to measure calcium signals of DA terminals in the NAcLat and dNAcMed (Figure 4A). Both terminals showed increased activity at the termination of restraint (Figures 4B, 4C, S4C, and S4D). Interestingly, while the stress relief CPP score did not correlate with calcium activities of VTA-DA somata (Figures S5A and S5B), probably due to heterogeneity, it did positively correlate with calcium activities of DA terminals in both the NAcLat and dNAcMed (Figures 4D–4G), suggesting that DA projections to the NAcLat and dNAcMed may specifically encode stress relief.

Using the genetically encoded G-protein-coupled receptor-activation-based DA ($GRAB_{DA}$) sensor, DA2m,[72] we found that, consistent with the calcium activity of DA neurons, at the termination of restraint stress, DA levels at the NAcLat and dNAcMed sites were also significantly increased (Figures 4H–4J), lasting for 23.9 s at the NAcLat (Figure S4E)

Please cite this article in press as: Dong et al., Stress relief as a natural resilience mechanism against depression-like behaviors, Neuron (2023), https://doi.org/10.1016/j.neuron.2023.09.004

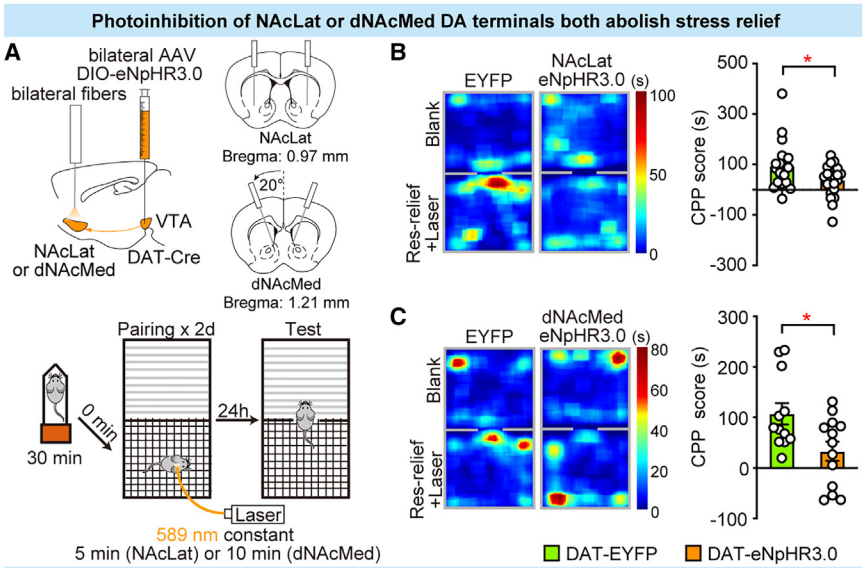

Figure 5. Photoinhibition of NAcLat or dNAcMed DA terminals blocks stress relief and facilitates despair- or anhedonia-like phenotypes, respectively

(A) Schematics of photoinhibiting NAcLat or dNAcMed DA terminals (top) and corresponding behavioral schematics of Res-relief CPP (bottom).

(B and C) Example heatmaps of Res-relief CPP with NAcLat (B) or dNAcMed (C) photoinhibition (left) and quantification of CPP score (right).

(D and H) Behavioral schematics of photoinhibiting NAcLat (D) or dNAcMed (H) DA terminals after terminating daily restraint during subthreshold 3-day CRS.

(E–G and I–K) Depression-like phenotypes in FST (E, F, I, and J) and SPT (G and K).

n.s., not significant; *p < 0.05; data represent mean ± SEM.

See also Figures S1 and S7 and Table S1.

and for 599.1 s at the dNAcMed (Figure S4F). When we went further downstream to monitor the calcium signals of D1R-expressing medium spiny neurons (D1-MSNs) at both sites (Figure S6A, top), the activity persisted even longer, lasting for 15 min at the NAcLat (Figure S6B) and >30 min at the dNAcMed (Figure S6C), suggesting that the G-protein-coupled receptor (GPCR) signaling of D1R may extend the action duration of DA.

DA projections to NAcLat and dNAcMed mediate stress relief to prevent distinct aspects of depression-like phenotypes

We next applied high-spatiotemporal manipulations to determine whether there are projection-specific effects on stress relief and depression resilience. We utilized eNpHR3.0[73] for bilateral photoinhibition of DA terminals in the NAcLat or dNAcMed, solely during the 5–10 min stress relief period (Figure 5A). Inhibition of either site abolished Res-relief CPP (Figures 5B and 5C). We then tried to inhibit either of these two pathways during the relief period right after daily restraint in a subthreshold 3-day CRS protocol (Figures 5D and 5H), which normally does not induce depression (Figures S3A–S3C). Intriguingly, photoinhibition of NAcLat DA terminals during stress relief specifically facilitated behavioral despair (Figures 5E–5G), whereas photoinhibition of dNAcMed DA terminals specifically facilitated anhedonia-like phenotypes (Figures 5I–5K). The above results reveal specific roles of the NAcLat and dNAcMed DA pathways during stress relief to counteract distinct aspects of depression-like phenotypes.

We next tested the inverse, to see whether we could prevent depression-like behaviors by enhancing relief reward through stimulating these two DA pathways. We photostimulated either pathway within the relief time window in a regular 14-day CRS model of depression (Figure 6A). Photostimulation of the NAcLat or dNAcMed DA terminals resulted in robust real-time place preference (Figures 6B–6D), mimicking the appetitive valence of stress relief. We then photostimulated either of these terminals for 5–10 min right after terminating the daily restraint during the 14-day CRS model of depression (Figures 6E and 6I). Notably, photostimulation of NAcLat DA terminals was sufficient to rescue both behavioral despair (Figures 6F and 6G) and anhedonia-like phenotypes (Figure 6H), whereas photostimulation of dNAcMed DA terminals only reversed anhedonia-like phenotypes (Figures 6J–6L). These results further confirmed the function of VTA-NAcLat and -dNAcMed DA pathways during stress relief in promoting resilience.

Please cite this article in press as: Dong et al., Stress relief as a natural resilience mechanism against depression-like behaviors, Neuron (2023), https://doi.org/10.1016/j.neuron.2023.09.004

CellPress

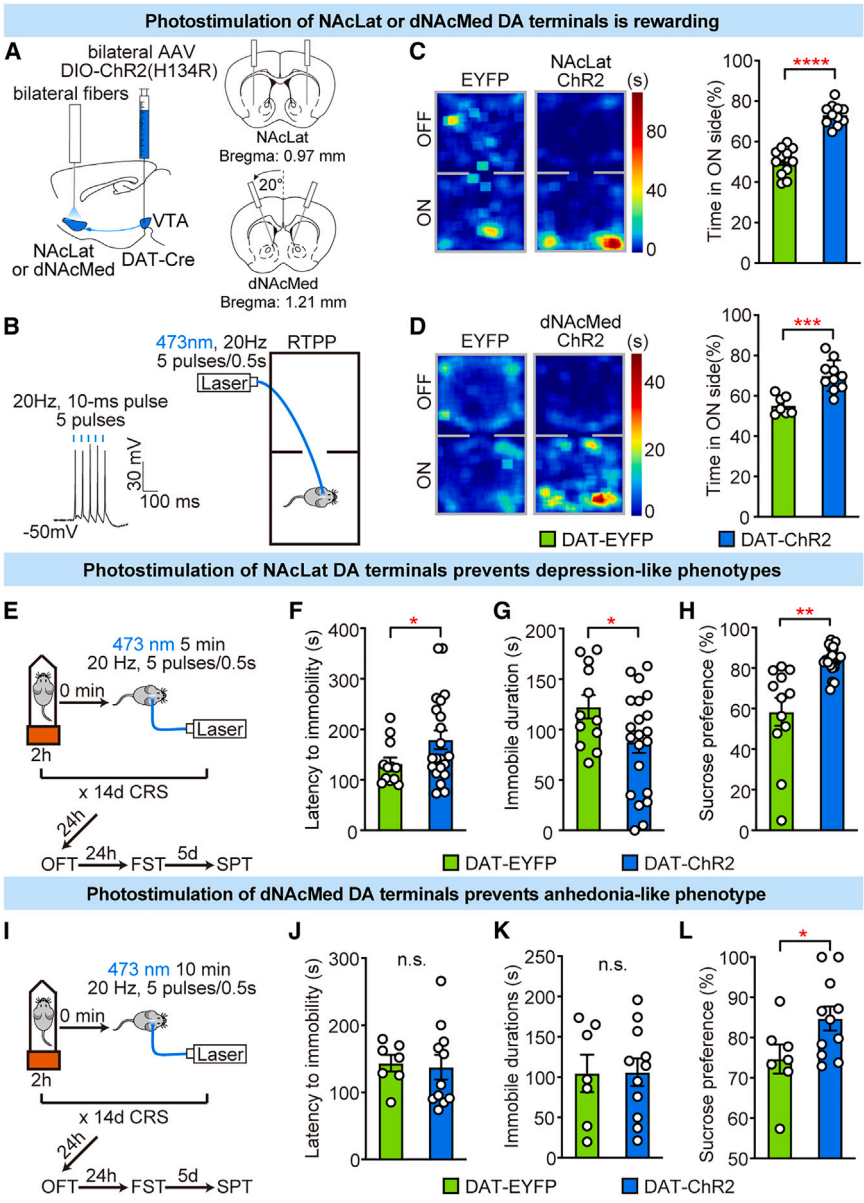

Figure 6. Photostimulation of NAcLat or dNAcMed DA terminals prevents depression-like phenotypes

(A) Schematics of photostimulating NAcLat or dNAcMed DA terminals.

(B) Example trace of light-evoked 20-Hz firings in VTA-DA neurons in slice recordings (left) and behavioral schematics of real-time place preference (RTPP) (right).

(C and D) Example RTPP heatmaps with NAcLat (C) or dNAcMed (D) photostimulation (left) and quantification of RTPP (right).

(E and I) Behavioral schematics of photostimulating NAcLat (E) or dNAcMed (I) DA terminals after terminating daily restraint during 14-day CRS.

(F–H and J–L) Depression-like phenotypes in FST (F, G, J, and K) and SPT (H and L).

n.s., not significant; $^{*}p < 0.05$, $^{**}p < 0.01$, $^{***}p < 0.001$, $^{****}p < 0.0001$; data represent mean ± SEM.

See also Figures S1 and S7 and Table S1.

level comparable to the naive group (Figures 7B–7D). In the second set of experiments, we reduced the duration of reward supply to 2 h (Figure 7E), and found that this shorter duration of no-delay reward was still sufficient to prevent depression-like phenotypes, whereas the 2-h delayed reward did not (Figures 7F–7H). Collectively, these results suggested that providing natural rewards shortly after stress termination to amplify the appetitive valence may be a promising behavioral strategy to enhance resilience to depression-like behaviors.

DISCUSSION

Here, we show that at the termination of physical stress, mice are transiently in a positively valenced relief state. Such a state depends on the activity of VTA-DA neurons and their projections to the NAcLat and dNAcMed, which are persistently activated during the relief period. Interestingly, the magnitude of stress relief strongly correlates with individual resilience to depression-like behaviors. Inhibition of stress relief facilitates depression-like behaviors, whereas a boost of stress relief prevents depression-like behaviors. Importantly, providing natural rewards within a critical window after stress promotes stress resilience, suggesting a non-invasive behavioral strategy to prevent depression.

A non-invasive behavioral strategy to prevent depression-like behaviors

Although optogenetics-based approaches demonstrated the necessity and sufficiency of DA pathways in encoding stress relief and promoting depression resilience, we wanted to see whether a non-invasive behavioral strategy to enhance stress relief could boost resilience. For this purpose, we tried to provide mice with natural rewards (*ad libitum* chocolate plus 2% sucrose water) after daily stress termination. In the first set of experiments, during the 14-day CRS induction, natural rewards were provided until the next day, either with (delayed reward group) or without (no-delay reward group) a 2-h delay after daily restraint (Figure 7A). Compared with either the no reward or the delayed reward group, the no-delay reward group showed much alleviated depression-like phenotypes in the FST and SPT, in a

Relief as a homeostatic defense mechanism for mood regulation

What is the benefit to have an emotional state of relief? Richard Solomon's opponent-process theory of motivation proposed that an opponent process after a significant departure from

Please cite this article in press as: Dong et al., Stress relief as a natural resilience mechanism against depression-like behaviors, Neuron (2023), https://doi.org/10.1016/j.neuron.2023.09.004

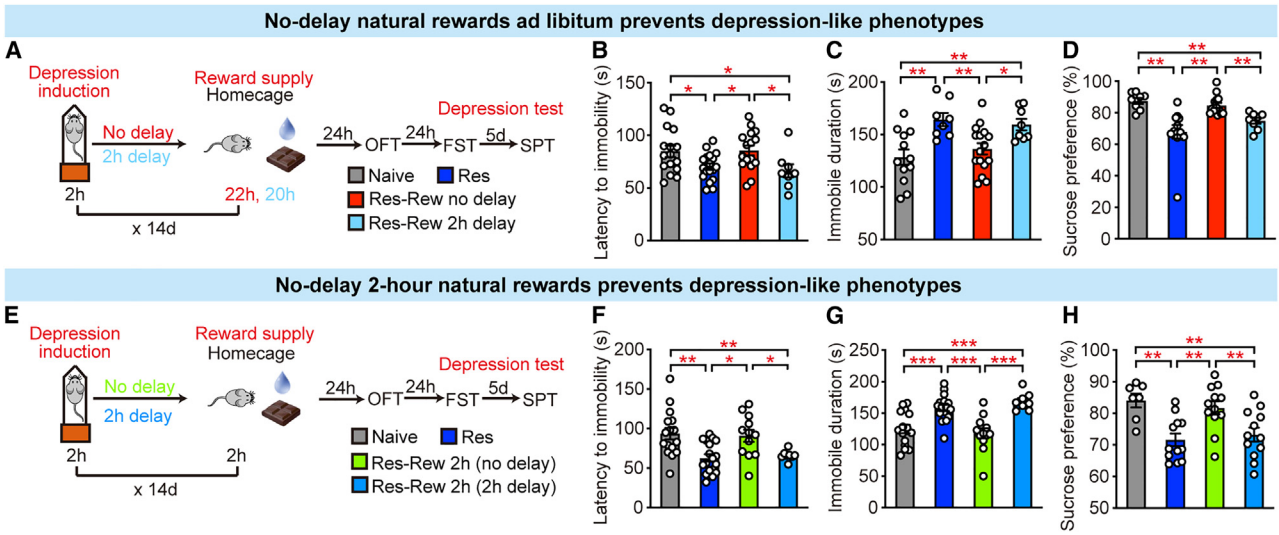

Figure 7. A non-invasive behavioral strategy to promote resilience

(A) Behavioral schematics of enhancing relief reward by supplying natural rewards (chocolate plus 2% sucrose *ad libitum*), with or without 2-h delay after terminating daily restraint during 14-day CRS.

(B–D) Depression-like phenotypes in FST (B and C) and SPT (D).

(E) Behavioral schematics of enhancing relief reward by supplying 2-h natural rewards, with or without a 2-h delay after daily restraint during 14-day CRS.

(F–H) Depression-like phenotypes in FST (F and G) and SPT (H).

*p < 0.05, **p < 0.01, ***p < 0.001; data represent mean ± SEM.

See also Figure S1 and Table S1.

affective equilibrium may serve a homeostatic defense function.[6,74] In the case of stress relief, during extended stress, activity of the reward-coding DA neurons is suppressed for a prolonged period of time (Figure 3J).[45,75,76] By having a surge in VTA-DA activity right after stress, organisms may self-compensate for the damaging effects resulting from stress-induced DA falloff. Therefore, relief may serve as an evolutionarily selected coping mechanism to insulate animals from the detrimental effects of stress. This proposition is supported by the correlation we observe between relief magnitude and resilience level, and the manipulation experiments showing that blocking or enhancing a relief reward prevents or promotes depression resilience, respectively. Notably, it remains unclear whether sex differences impact on this relief mechanism. As we performed experiments only in male mice, future investigations are warranted as to whether and how female mice also utilize relief for mood regulation.

VTA-DA heterogeneity in stress relief

VTA-DA projections to different downstream areas have been demonstrated to define DA heterogeneity in a wide range of physiological and pathological conditions.[77,78] Adding to this general theme of VTA-DA heterogeneity, our results identified distinct profiles of calcium activity in dissociable VTA-DA pathways during stress relief. After stress termination, DA projections to the NAcLat are transiently activated for about 6 s (Figure 4B), whereas DA projections to the dNAcMed show more persistent activation for 9 min (Figure S4B). Monitoring of DA release in the NAcLat and dNAcMed further confirmed such distinct temporal dynamics (Figures S4C and S4D).

On the other hand, when we monitored calcium activities of the neural targets of the above two pathways, D1-MSNs in the NAcLat and dNAcMed, there were persistent activities lasting for more than 15 min in both pathways (Figure S6). This suggests that D1R signaling extends the duration of action of DA, possibly through cyclic adenosine monophosphate (cAMP) and protein kinase A (PKA) pathways.[79,80]

Functional divergence of VTA-NAcLat and -dNAcMed DA pathways in depression resilience

Recent studies suggest that disparate depression-like phenotypes are encoded within discrete neural circuits.[81–83] For example, social withdrawal and behavioral despair phenotypes are separately embedded in VTA-projecting and lateral habenula-projecting ventral pallidum neurons, respectively.[81] Here, we found that photoinhibition of the NAcLat and dNAcMed DA terminals right after stress facilitates behavioral despair and anhedonia-like phenotypes, respectively, in a subthreshold chronic stress model of depression (Figures 5D–5K). This suggests that the activities of these two DA pathways during the relief period are normally required to combat the two distinct depression-like phenotypes.

On the other hand, while photostimulation of dNAcMed DA terminals during relief periods specifically rescued anhedonia-like phenotypes (Figures 6I–6L), photostimulation of NAcLat DA terminals ameliorated both despair- and anhedonia-like phenotypes (Figures 6E–6H). The incongruence in the manipulation results of NAcLat may be explained by the fact that D1-MSNs in the NAcLat, but not dNAcMed, predominantly inhibit VTA γ-aminobutyric acid (GABA) neurons.[84] Therefore, by inhibiting

VTA-GABA neurons, photostimulation of NAcLat DA terminals can lead to the disinhibition of VTA-DA neurons, which innervates both the NAcLat and dNAcMed, affecting both depression-like phenotypes. Consistent with this postulation, chemogenetic activation of D1-MSNs in the NAcLat,[85] or photoinhibition of VTA-GABA neurons, reverses anhedonia-like phenotypes.[86] Furthermore, because NAc MSNs remain silent in the absence of reward stimuli,[87] the lack of tonic inhibition onto VTA-GABA neurons may explain why photoinhibition of the VTA-NAcLat DA pathway did not facilitate anhedonia-like phenotypes (Figure 5G).

Possible neural mechanisms mediating the persistent DA activity

The minute-long activation of VTA-DA neurons after stress termination raises the question of what neural mechanisms may mediate such persistent activity. Local neuronal intrinsic properties and upstream inputs,[88,89] as well as neuropeptides (such as enkephalin, dynorphin, nociceptin, etc.),[90–93] are three potential mechanisms that can be tested in the future. In terms of intrinsic properties, VTA-DA neurons contain T-type calcium channels, which can support rebound firings after inhibition.[94] Given that a good portion of VTA-DA neurons are inhibited by aversive stimuli,[45,75,76] it would be interesting to test whether the rebound excitation after inhibition can last minutes long to account for the persistent activity during stress relief. Alternatively, upstream excitatory or inhibitory inputs onto the VTA-DA neurons may undergo persistent activation or inhibition during the relief and thus convey the signals to VTA-DA neurons. This may be tested by recording and screening through local (e.g., VTA-glutamatergic[95] and VTA-GABAergic neurons[84,96–98]) and upstream inputs (e.g., rostromedial tegmental nucleus,[99,100] laterodorsal tegmental nucleus,[60,101] dorsal raphe,[23,102] anterior cortex,[103] and pedunculopontine tegmental nucleus[104,105]).

Augmentation of relief reward as a behavioral strategy to promote resilience

Here, we propose a new behavioral strategy to promote depression resilience by providing natural rewards right after stress termination. This strategy is different from another relief-based protocol, called "learned safety," which requires repeated pairings with a neutral "safety" signal.[106] We map the optimal time window for supplying natural rewards to be within 2 h of stress termination. This hour-level time window is longer than that of the relief window (<10 min) mapped by CPP (Figure 1G) or the duration of VTA-DA activation (Figure 3C). This difference could be due to the detection sensitivity of CPP and photometry measurements. Alternatively, it may indicate that the effective time window for interventions is longer than that of the endogenous relief mechanism. Either way, a 2-h window after stress makes this behavioral strategy more implementable. In terms of choice of reward, although we used chocolate and sucrose water in this study, other types of natural reward—especially social reward—should also be explored, given that social reward also activates the VTA-NAc DA pathway[67] and that activating positive memory of social reward alleviates depression-like behaviors.[107] Previous findings have explored the analgesic function of pain relief.[17,108,109] We hope the current study may shed light on harnessing the antidepressant function of stress relief.

STAR★METHODS

Detailed methods are provided in the online version of this paper and include the following:

- KEY RESOURCES TABLE
- RESOURCE AVAILABILITY
  - Lead contact
  - Materials availability
  - Data and code availability
- EXPERIMENTAL MODEL AND STUDY PARTICIPANT DETAILS
  - Animals
- METHOD DETAILS
  - Drugs and treatments
  - Stereotaxic surgeries
  - Optogenetic stimulation assays
  - Behavioral assays
  - Open field test
  - Elevated plus maze test
  - Novelty-suppressed feeding test
  - Forced swim test
  - Sucrose preference test
  - Real time place preference
  - Fiber photometry
  - *In vitro* electrophysiology
  - *In vivo* optrode recording in freely moving mice
  - Histological verifications and immunohistochemistry
- QUANTIFICATION AND STATISTICAL ANALYSIS

SUPPLEMENTAL INFORMATION

Supplemental information can be found online at https://doi.org/10.1016/j.neuron.2023.09.004.

ACKNOWLEDGMENTS

We thank Shuqi Chen, Yongli Gao, Xiao Guo, and Tingting Zhou for preliminary explorations; Jihua Wang, Long Li, and Xiaochun Jiang for help in fiber photometry; Hongbin Yang, Zhaoqi Dong, and Yue Li for manuscript discussion; Fangmiao Sun for advice on dopamine sensors; and Yao Wang and Sen Jin for advice on AAVs. Some graphic components were created with BioRender. This work was supported by the STI2030-Major Projects (2021ZD0203000 and 2021ZD0203001), the National Natural Science Foundation of China (32130042, 31830032, and 82288101), the Key-Area Research and Development Program of Guangdong Province (2018B030334001 and 2018B030331001), the National Key Research and Development Program of China (2016YFA0501000), the Starry Night Science Fund of Zhejiang University Shanghai Institute for Advanced Study (SN-ZJU-SIAS-002), and the New Cornerstone Science Foundation to H.H.

AUTHOR CONTRIBUTIONS

H.H. and Y.D. designed the study; Y.D. and Yifei Li performed fiber photometry with the help of J.H.; Y.D. and Yifei Li performed optogenetic manipulations and behavioral tests; Y.D. and X.X. performed *in vivo* optrode recording under the supervision of H.L. and H.H.; H.H., Y.D., Yifei Li, X.X., Z.-C.X., and H.L. analyzed data; Yulong Li shared dopamine sensors; Z.-C.X. contributed to discussions; and H.H. and Y.D. wrote the manuscript with the help of Yifei Li.

DECLARATION OF INTERESTS

H.H. is a member of the advisory board of *Neuron*.

Received: November 28, 2022
Revised: August 7, 2023
Accepted: September 6, 2023
Published: September 29, 2023

REFERENCES

1. Anderson, D.J., and Adolphs, R. (2014). A framework for studying emotions across species. Cell *157*, 187–200. https://doi.org/10.1016/j.cell.2014.03.003.
2. Xiu, J., Zhang, Q., Zhou, T., Zhou, T.T., Chen, Y., and Hu, H. (2014). Visualizing an emotional valence map in the limbic forebrain by TAI-FISH. Nat. Neurosci. *17*, 1552–1559. https://doi.org/10.1038/nn.3813.
3. Hu, H. (2016). Reward and aversion. Annu. Rev. Neurosci. *39*, 297–324. https://doi.org/10.1146/annurev-neuro-070815-014106.
4. Tye, K.M. (2018). Neural circuit motifs in valence processing. Neuron *100*, 436–452. https://doi.org/10.1016/j.neuron.2018.10.001.
5. Berridge, K.C. (2019). Affective valence in the brain: modules or modes? Nat. Rev. Neurosci. *20*, 225–234. https://doi.org/10.1038/s41583-019-0122-8.
6. Solomon, R.L., and Corbit, J.D. (1974). An opponent-process theory of motivation. I. Temporal dynamics of affect. Psychol. Rev. *81*, 119–145. https://doi.org/10.1037/h0036128.
7. Koob, G.F., and Le Moal, M. (1997). Drug abuse: hedonic homeostatic dysregulation. Science *278*, 52–58. https://doi.org/10.1126/science.278.5335.52.
8. Koob, G.F. (2020). Neurobiology of opioid addiction: opponent process, hyperkatifeia, and negative reinforcement. Biol. Psychiatry *87*, 44–53. https://doi.org/10.1016/j.biopsych.2019.05.023.
9. Fowler, C.D., Lu, Q., Johnson, P.M., Marks, M.J., and Kenny, P.J. (2011). Habenular α5 nicotinic receptor subunit signalling controls nicotine intake. Nature *471*, 597–601. https://doi.org/10.1038/nature09797.
10. Meye, F.J., Valentinova, K., Lecca, S., Marion-Poll, L., Maroteaux, M.J., Musardo, S., Moutkine, I., Gardoni, F., Huganir, R.L., Georges, F., et al. (2015). Cocaine-evoked negative symptoms require AMPA receptor trafficking in the lateral habenula. Nat. Neurosci. *18*, 376–378. https://doi.org/10.1038/nn.3923.
11. Zhu, Y., Wienecke, C.F., Nachtrab, G., and Chen, X. (2016). A thalamic input to the nucleus accumbens mediates opiate dependence. Nature *530*, 219–222. https://doi.org/10.1038/nature16954.
12. Tanimoto, H., Heisenberg, M., and Gerber, B. (2004). Experimental psychology: event timing turns punishment to reward. Nature *430*, 983. https://doi.org/10.1038/430983a.
13. Seymour, B., O'Doherty, J.P., Koltzenburg, M., Wiech, K., Frackowiak, R., Friston, K., and Dolan, R. (2005). Opponent appetitive-aversive neural processes underlie predictive learning of pain relief. Nat. Neurosci. *8*, 1234–1240. https://doi.org/10.1038/nn1527.
14. Gerber, B., Yarali, A., Diegelmann, S., Wotjak, C.T., Pauli, P., and Fendt, M. (2014). Pain-relief learning in flies, rats, and man: basic research and applied perspectives. Learn. Mem. *21*, 232–252. https://doi.org/10.1101/lm.032995.113.
15. Shen, Y.L., Chen, Y.C., and Liao, R.M. (2010). Dopamine receptor antagonists impair place conditioning after acute stress in rats. Behav. Pharmacol. *21*, 77–82. https://doi.org/10.1097/FBP.0b013e3283359f20.
16. Rogan, M.T., Leon, K.S., Perez, D.L., and Kandel, E.R. (2005). Distinct neural signatures for safety and danger in the amygdala and striatum of the mouse. Neuron *46*, 309–320. https://doi.org/10.1016/j.neuron.2005.02.017.
17. Navratilova, E., Xie, J.Y., Okun, A., Qu, C., Eyde, N., Ci, S., Ossipov, M.H., King, T., Fields, H.L., and Porreca, F. (2012). Pain relief produces negative reinforcement through activation of mesolimbic reward-valuation circuitry. Proc. Natl. Acad. Sci. USA *109*, 20709–20713. https://doi.org/10.1073/pnas.1214605109.
18. Mohammadi, M., Bergado-Acosta, J.R., and Fendt, M. (2014). Relief learning is distinguished from safety learning by the requirement of the nucleus accumbens. Behav. Brain Res. *272*, 40–45. https://doi.org/10.1016/j.bbr.2014.06.053.
19. Bergado Acosta, J.R., Kahl, E., Kogias, G., Uzuneser, T.C., and Fendt, M. (2017). Relief learning requires a coincident activation of dopamine D1 and NMDA receptors within the nucleus accumbens. Neuropharmacology *114*, 58–66. https://doi.org/10.1016/j.neuropharm.2016.11.022.
20. Luo, R., Uematsu, A., Weitemier, A., Aquili, L., Koivumaa, J., McHugh, T.J., and Johansen, J.P. (2018). A dopaminergic switch for fear to safety transitions. Nat. Commun. *9*, 2483. https://doi.org/10.1038/s41467-018-04784-7.
21. Salinas-Hernández, X.I., Vogel, P., Betz, S., Kalisch, R., Sigurdsson, T., and Duvarci, S. (2018). Dopamine neurons drive fear extinction learning by signaling the omission of expected aversive outcomes. eLife *7*. https://doi.org/10.7554/eLife.38818.
22. Cai, L.X., Pizano, K., Gundersen, G.W., Hayes, C.L., Fleming, W.T., Holt, S., Cox, J.M., and Witten, I.B. (2020). Distinct signals in medial and lateral VTA dopamine neurons modulate fear extinction at different times. eLife *9*. https://doi.org/10.7554/eLife.54936.
23. de Jong, J.W., Afjei, S.A., Pollak Dorocic, I., Peck, J.R., Liu, C., Kim, C.K., Tian, L., Deisseroth, K., and Lammel, S. (2019). A neural circuit mechanism for encoding aversive stimuli in the mesolimbic dopamine system. Neuron *101*, 133–151.e7. https://doi.org/10.1016/j.neuron.2018.11.005.
24. Su, X.Y., Chen, M., Yuan, Y., Li, Y., Guo, S.S., Luo, H.Q., Huang, C., Sun, W., Li, Y., Zhu, M.X., et al. (2019). Central processing of itch in the midbrain reward center. Neuron *102*, 858–872.e5. https://doi.org/10.1016/j.neuron.2019.03.030.
25. Rutter, M. (1985). Resilience in the face of adversity. Protective factors and resistance to psychiatric disorder. Br. J. Psychiatry *147*, 598–611. https://doi.org/10.1192/bjp.147.6.598.
26. Charney, D.S. (2004). Psychobiological mechanisms of resilience and vulnerability: implications for successful adaptation to extreme stress. Am. J. Psychiatry *161*, 195–216. https://doi.org/10.1176/appi.ajp.161.2.195.
27. Cathomas, F., Murrough, J.W., Nestler, E.J., Han, M.H., and Russo, S.J. (2019). Neurobiology of resilience: interface between mind and body. Biol. Psychiatry *86*, 410–420. https://doi.org/10.1016/j.biopsych.2019.04.011.
28. Russo, S.J., Murrough, J.W., Han, M.H., Charney, D.S., and Nestler, E.J. (2012). Neurobiology of resilience. Nat. Neurosci. *15*, 1475–1484. https://doi.org/10.1038/nn.3234.
29. Cui, Y., Huang, X., Huang, P., Huang, L., Feng, Z., Xiang, X., Chen, X., Li, A., Ren, C., and Li, H. (2022). Reward ameliorates depressive-like behaviors via inhibition of the substantia innominata to the lateral habenula projection. Sci. Adv. *8*, eabn0193. https://doi.org/10.1126/sciadv.abn0193.
30. Krishnan, V., Han, M.H., Graham, D.L., Berton, O., Renthal, W., Russo, S.J., Laplant, Q., Graham, A., Lutter, M., Lagace, D.C., et al. (2007). Molecular adaptations underlying susceptibility and resistance to social defeat in brain reward regions. Cell *131*, 391–404. https://doi.org/10.1016/j.cell.2007.09.018.
31. Dias, C., Feng, J., Sun, H., Shao, N.Y., Mazei-Robison, M.S., Damez-Werno, D., Scobie, K., Bagot, R., LaBonté, B., Ribeiro, E., et al. (2014). Beta-catenin mediates stress resilience through Dicer1/microRNA regulation. Nature *516*, 51–55. https://doi.org/10.1038/nature13976.
32. Francis, T.C., Chandra, R., Friend, D.M., Finkel, E., Dayrit, G., Miranda, J., Brooks, J.M., Iñiguez, S.D., O'Donnell, P., Kravitz, A., et al. (2015). Nucleus accumbens medium spiny neuron subtypes mediate

depression-related outcomes to social defeat stress. Biol. Psychiatry *77*, 212–222. https://doi.org/10.1016/j.biopsych.2014.07.021.

33. Anacker, C., Luna, V.M., Stevens, G.S., Millette, A., Shores, R., Jimenez, J.C., Chen, B., and Hen, R. (2018). Hippocampal neurogenesis confers stress resilience by inhibiting the ventral dentate gyrus. Nature *559*, 98–102. https://doi.org/10.1038/s41586-018-0262-4.
34. Tye, K.M., Mirzabekov, J.J., Warden, M.R., Ferenczi, E.A., Tsai, H.C., Finkelstein, J., Kim, S.Y., Adhikari, A., Thompson, K.R., Andalman, A.S., et al. (2013). Dopamine neurons modulate neural encoding and expression of depression-related behaviour. Nature *493*, 537–541. https://doi.org/10.1038/nature11740.
35. Chaudhury, D., Walsh, J.J., Friedman, A.K., Juarez, B., Ku, S.M., Koo, J.W., Ferguson, D., Tsai, H.C., Pomeranz, L., Christoffel, D.J., et al. (2013). Rapid regulation of depression-related behaviours by control of midbrain dopamine neurons. Nature *493*, 532–536. https://doi.org/10.1038/nature11713.
36. Friedman, A.K., Walsh, J.J., Juarez, B., Ku, S.M., Chaudhury, D., Wang, J., Li, X., Dietz, D.M., Pan, N., Vialou, V.F., et al. (2014). Enhancing depression mechanisms in midbrain dopamine neurons achieves homeostatic resilience. Science *344*, 313–319. https://doi.org/10.1126/science.1249240.
37. Isingrini, E., Perret, L., Rainer, Q., Amilhon, B., Guma, E., Tanti, A., Martin, G., Robinson, J., Moquin, L., Marti, F., et al. (2016). Resilience to chronic stress is mediated by noradrenergic regulation of dopamine neurons. Nat. Neurosci. *19*, 560–563. https://doi.org/10.1038/nn.4245.
38. Willmore, L., Cameron, C., Yang, J., Witten, I.B., and Falkner, A.L. (2022). Behavioural and dopaminergic signatures of resilience. Nature *611*, 124–132. https://doi.org/10.1038/s41586-022-05328-2.
39. Mucha, R.F., van der Kooy, D., O'Shaughnessy, M., and Bucenieks, P. (1982). Drug reinforcement studied by the use of place conditioning in rat. Brain Res. *243*, 91–105. https://doi.org/10.1016/0006-8993(82)91123-4.
40. Cunningham, C.L., Gremel, C.M., and Groblewski, P.A. (2006). Drug-induced conditioned place preference and aversion in mice. Nat. Protoc. *1*, 1662–1670. https://doi.org/10.1038/nprot.2006.279.
41. Kim, K.S., and Han, P.L. (2006). Optimization of chronic stress paradigms using anxiety- and depression-like behavioral parameters. J. Neurosci. Res. *83*, 497–507. https://doi.org/10.1002/jnr.20754.
42. Yang, Y., Cui, Y., Sang, K., Dong, Y., Ni, Z., Ma, S., and Hu, H. (2018). Ketamine blocks bursting in the lateral habenula to rapidly relieve depression. Nature *554*, 317–322. https://doi.org/10.1038/nature25509.
43. Coddington, L.T., and Dudman, J.T. (2019). Learning from action: reconsidering movement signaling in midbrain dopamine neuron activity. Neuron *104*, 63–77. https://doi.org/10.1016/j.neuron.2019.08.036.
44. Berke, J.D. (2018). What does dopamine mean? Nat. Neurosci. *21*, 787–793. https://doi.org/10.1038/s41593-018-0152-y.
45. Cohen, J.Y., Haesler, S., Vong, L., Lowell, B.B., and Uchida, N. (2012). Neuron-type-specific signals for reward and punishment in the ventral tegmental area. Nature *482*, 85–88. https://doi.org/10.1038/nature10754.
46. Hughes, R.N., Bakhurin, K.I., Petter, E.A., Watson, G.D.R., Kim, N., Friedman, A.D., and Yin, H.H. (2020). Ventral tegmental dopamine neurons control the impulse vector during motivated behavior. Curr. Biol. *30*, 2681–2694.e5. https://doi.org/10.1016/j.cub.2020.05.003.
47. Schultz, W. (2016). Dopamine reward prediction-error signalling: a two-component response. Nat. Rev. Neurosci. *17*, 183–195. https://doi.org/10.1038/nrn.2015.26.
48. Bromberg-Martin, E.S., Matsumoto, M., and Hikosaka, O. (2010). Dopamine in motivational control: rewarding, aversive, and alerting. Neuron *68*, 815–834. https://doi.org/10.1016/j.neuron.2010.11.022.
49. Watabe-Uchida, M., Eshel, N., and Uchida, N. (2017). Neural circuitry of reward prediction error. Annu. Rev. Neurosci. *40*, 373–394. https://doi.org/10.1146/annurev-neuro-072116-031109.
50. Brischoux, F., Chakraborty, S., Brierley, D.I., and Ungless, M.A. (2009). Phasic excitation of dopamine neurons in ventral VTA by noxious stimuli. Proc. Natl. Acad. Sci. USA *106*, 4894–4899. https://doi.org/10.1073/pnas.0811507106.
51. Zweifel, L.S., Fadok, J.P., Argilli, E., Garelick, M.G., Jones, G.L., Dickerson, T.M., Allen, J.M., Mizumori, S.J., Bonci, A., and Palmiter, R.D. (2011). Activation of dopamine neurons is critical for aversive conditioning and prevention of generalized anxiety. Nat. Neurosci. *14*, 620–626. https://doi.org/10.1038/nn.2808.
52. Chang, C.Y., Esber, G.R., Marrero-Garcia, Y., Yau, H.J., Bonci, A., and Schoenbaum, G. (2016). Brief optogenetic inhibition of dopamine neurons mimics endogenous negative reward prediction errors. Nat. Neurosci. *19*, 111–116. https://doi.org/10.1038/nn.4191.
53. Tsai, H.C., Zhang, F., Adamantidis, A., Stuber, G.D., Bonci, A., de Lecea, L., and Deisseroth, K. (2009). Phasic firing in dopaminergic neurons is sufficient for behavioral conditioning. Science *324*, 1080–1084. https://doi.org/10.1126/science.1168878.
54. Pignatelli, M., and Bonci, A. (2015). Role of dopamine neurons in reward and aversion: a synaptic plasticity perspective. Neuron *86*, 1145–1157. https://doi.org/10.1016/j.neuron.2015.04.015.
55. Lammel, S., Hetzel, A., Häckel, O., Jones, I., Liss, B., and Roeper, J. (2008). Unique properties of mesoprefrontal neurons within a dual mesocorticolimbic dopamine system. Neuron *57*, 760–773. https://doi.org/10.1016/j.neuron.2008.01.022.
56. Lammel, S., Lim, B.K., and Malenka, R.C. (2014). Reward and aversion in a heterogeneous midbrain dopamine system. Neuropharmacology *76*, 351–359. https://doi.org/10.1016/j.neuropharm.2013.03.019.
57. Farassat, N., Costa, K.M., Stojanovic, S., Albert, S., Kovacheva, L., Shin, J., Egger, R., Somayaji, M., Duvarci, S., Schneider, G., et al. (2019). In vivo functional diversity of midbrain dopamine neurons within identified axonal projections. eLife *8*. https://doi.org/10.7554/eLife.48408.
58. Margolis, E.B., Lock, H., Chefer, V.I., Shippenberg, T.S., Hjelmstad, G.O., and Fields, H.L. (2006). Kappa opioids selectively control dopaminergic neurons projecting to the prefrontal cortex. Proc. Natl. Acad. Sci. USA *103*, 2938–2942. https://doi.org/10.1073/pnas.0511159103.
59. Lammel, S., Ion, D.I., Roeper, J., and Malenka, R.C. (2011). Projection-specific modulation of dopamine neuron synapses by aversive and rewarding stimuli. Neuron *70*, 855–862. https://doi.org/10.1016/j.neuron.2011.03.025.
60. Lammel, S., Lim, B.K., Ran, C., Huang, K.W., Betley, M.J., Tye, K.M., Deisseroth, K., and Malenka, R.C. (2012). Input-specific control of reward and aversion in the ventral tegmental area. Nature *491*, 212–217. https://doi.org/10.1038/nature11527.
61. Nguyen, C., Mondoloni, S., Le Borgne, T., Centeno, I., Come, M., Jehl, J., Solié, C., Reynolds, L.M., Durand-de Cuttoli, R., Tolu, S., et al. (2021). Nicotine inhibits the VTA-to-amygdala dopamine pathway to promote anxiety. Neuron *109*, 2604–2615.e9. https://doi.org/10.1016/j.neuron.2021.06.013.
62. Lutas, A., Kucukdereli, H., Alturkistani, O., Carty, C., Sugden, A.U., Fernando, K., Diaz, V., Flores-Maldonado, V., and Andermann, M.L. (2019). State-specific gating of salient cues by midbrain dopaminergic input to basal amygdala. Nat. Neurosci. *22*, 1820–1833. https://doi.org/10.1038/s41593-019-0506-0.
63. Vander Weele, C.M., Siciliano, C.A., Matthews, G.A., Namburi, P., Izadmehr, E.M., Espinel, I.C., Nieh, E.H., Schut, E.H.S., Padilla-Coreano, N., Burgos-Robles, A., et al. (2018). Dopamine enhances signal-to-noise ratio in cortical-brainstem encoding of aversive stimuli. Nature *563*, 397–401. https://doi.org/10.1038/s41586-018-0682-1.
64. Jo, Y.S., Heymann, G., and Zweifel, L.S. (2018). Dopamine neurons reflect the uncertainty in fear generalization. Neuron *100*, 916–925.e3. https://doi.org/10.1016/j.neuron.2018.09.028.
65. Mohebi, A., Pettibone, J.R., Hamid, A.A., Wong, J.T., Vinson, L.T., Patriarchi, T., Tian, L., Kennedy, R.T., and Berke, J.D. (2019).

Dissociable dopamine dynamics for learning and motivation. Nature *570*, 65–70. https://doi.org/10.1038/s41586-019-1235-y.

66. Parker, N.F., Cameron, C.M., Taliaferro, J.P., Lee, J., Choi, J.Y., Davidson, T.J., Daw, N.D., and Witten, I.B. (2016). Reward and choice encoding in terminals of midbrain dopamine neurons depends on striatal target. Nat. Neurosci. *19*, 845–854. https://doi.org/10.1038/nn.4287.
67. Gunaydin, L.A., Grosenick, L., Finkelstein, J.C., Kauvar, I.V., Fenno, L.E., Adhikari, A., Lammel, S., Mirzabekov, J.J., Airan, R.D., Zalocusky, K.A., et al. (2014). Natural neural projection dynamics underlying social behavior. Cell *157*, 1535–1551. https://doi.org/10.1016/j.cell.2014.05.017.
68. Heymann, G., Jo, Y.S., Reichard, K.L., McFarland, N., Chavkin, C., Palmiter, R.D., Soden, M.E., and Zweifel, L.S. (2020). Synergy of distinct dopamine projection populations in behavioral reinforcement. Neuron *105*, 909–920.e5. https://doi.org/10.1016/j.neuron.2019.11.024.
69. Saunders, B.T., Richard, J.M., Margolis, E.B., and Janak, P.H. (2018). Dopamine neurons create Pavlovian conditioned stimuli with circuit-defined motivational properties. Nat. Neurosci. *21*, 1072–1083. https://doi.org/10.1038/s41593-018-0191-4.
70. Yuan, L., Dou, Y.N., and Sun, Y.G. (2019). Topography of reward and aversion encoding in the mesolimbic dopaminergic system. J. Neurosci. *39*, 6472–6481. https://doi.org/10.1523/JNEUROSCI.0271-19.2019.
71. Liu, C., Tose, A.J., Verharen, J.P.H., Zhu, Y., Tang, L.W., de Jong, J.W., Du, J.X., Beier, K.T., and Lammel, S. (2022). An inhibitory brainstem input to dopamine neurons encodes nicotine aversion. Neuron *110*, 3018–3035.e7. https://doi.org/10.1016/j.neuron.2022.07.003.
72. Sun, F., Zhou, J., Dai, B., Qian, T., Zeng, J., Li, X., Zhuo, Y., Zhang, Y., Wang, Y., Qian, C., et al. (2020). Next-generation GRAB sensors for monitoring dopaminergic activity in vivo. Nat. Methods *17*, 1156–1166. https://doi.org/10.1038/s41592-020-00981-9.
73. Gradinaru, V., Zhang, F., Ramakrishnan, C., Mattis, J., Prakash, R., Diester, I., Goshen, I., Thompson, K.R., and Deisseroth, K. (2010). Molecular and cellular approaches for diversifying and extending optogenetics. Cell *141*, 154–165. https://doi.org/10.1016/j.cell.2010.02.037.
74. Solomon, R.L. (1980). The opponent-process theory of acquired motivation: the costs of pleasure and the benefits of pain. Am. Psychol. *35*, 691–712. https://doi.org/10.1037/0003-066x.35.8.691.
75. Ungless, M.A., Magill, P.J., and Bolam, J.P. (2004). Uniform inhibition of dopamine neurons in the ventral tegmental area by aversive stimuli. Science *303*, 2040–2042. https://doi.org/10.1126/science.1093360.
76. Matsumoto, M., and Hikosaka, O. (2009). Two types of dopamine neuron distinctly convey positive and negative motivational signals. Nature *459*, 837–841. https://doi.org/10.1038/nature08028.
77. Verharen, J.P.H., Zhu, Y., and Lammel, S. (2020). Aversion hot spots in the dopamine system. Curr. Opin. Neurobiol. *64*, 46–52. https://doi.org/10.1016/j.conb.2020.02.002.
78. de Jong, J.W., Fraser, K.M., and Lammel, S. (2022). Mesoaccumbal dopamine heterogeneity: what do dopamine firing and release have to do with it? Annu. Rev. Neurosci. *45*, 109–129. https://doi.org/10.1146/annurev-neuro-110920-011929.
79. Lahiri, A.K., and Bevan, M.D. (2020). Dopaminergic transmission rapidly and persistently enhances excitability of D1 receptor-expressing striatal projection neurons. Neuron *106*, 277–290.e6. https://doi.org/10.1016/j.neuron.2020.01.028.
80. Zhang, S.X., Lutas, A., Yang, S., Diaz, A., Fluhr, H., Nagel, G., Gao, S., and Andermann, M.L. (2021). Hypothalamic dopamine neurons motivate mating through persistent cAMP signalling. Nature *597*, 245–249. https://doi.org/10.1038/s41586-021-03845-0.
81. Knowland, D., Lilascharoen, V., Pacia, C.P., Shin, S., Wang, E.H., and Lim, B.K. (2017). Distinct ventral pallidal neural populations mediate separate symptoms of depression. Cell *170*, 284–297.e18. https://doi.org/10.1016/j.cell.2017.06.015.
82. Cerniauskas, I., Winterer, J., de Jong, J.W., Lukacsovich, D., Yang, H., Khan, F., Peck, J.R., Obayashi, S.K., Lilascharoen, V., Lim, B.K., et al. (2019). Chronic stress induces activity, synaptic, and transcriptional remodeling of the lateral habenula associated with deficits in motivated behaviors. Neuron *104*, 899–915.e8. https://doi.org/10.1016/j.neuron.2019.09.005.
83. Lim, B.K., Huang, K.W., Grueter, B.A., Rothwell, P.E., and Malenka, R.C. (2012). Anhedonia requires MC4R-mediated synaptic adaptations in nucleus accumbens. Nature *487*, 183–189. https://doi.org/10.1038/nature11160.
84. Yang, H., de Jong, J.W., Tak, Y., Peck, J., Bateup, H.S., and Lammel, S. (2018). Nucleus accumbens subnuclei regulate motivated behavior via direct inhibition and disinhibition of VTA dopamine subpopulations. Neuron *97*, 434–449.e4. https://doi.org/10.1016/j.neuron.2017.12.022.
85. He, Z.X., Yin, Y.Y., Xi, K., Xing, Z.K., Cao, J.B., Liu, T.Y., Liu, L., He, X.X., Yu, H.L., and Zhu, X.J. (2020). Nucleus accumbens Tac1-expressing neurons mediate stress-induced anhedonia-like behavior in mice. Cell Rep. *33*, 108343. https://doi.org/10.1016/j.celrep.2020.108343.
86. Lowes, D.C., Chamberlin, L.A., Kretsge, L.N., Holt, E.S., Abbas, A.I., Park, A.J., Yusufova, L., Bretton, Z.H., Firdous, A., Enikolopov, A.G., et al. (2021). Ventral tegmental area GABA neurons mediate stress-induced blunted reward-seeking in mice. Nat. Commun. *12*, 3539. https://doi.org/10.1038/s41467-021-23906-2.
87. McGinty, V.B., Lardeux, S., Taha, S.A., Kim, J.J., and Nicola, S.M. (2013). Invigoration of reward seeking by cue and proximity encoding in the nucleus accumbens. Neuron *78*, 910–922. https://doi.org/10.1016/j.neuron.2013.04.010.
88. Stagkourakis, S., Spigolon, G., Williams, P., Protzmann, J., Fisone, G., and Broberger, C. (2018). A neural network for intermale aggression to establish social hierarchy. Nat. Neurosci. *21*, 834–842. https://doi.org/10.1038/s41593-018-0153-x.
89. Kennedy, A., Kunwar, P.S., Li, L.Y., Stagkourakis, S., Wagenaar, D.A., and Anderson, D.J. (2020). Stimulus-specific hypothalamic encoding of a persistent defensive state. Nature *586*, 730–734. https://doi.org/10.1038/s41586-020-2728-4.
90. Zelikowsky, M., Hui, M., Karigo, T., Choe, A., Yang, B., Blanco, M.R., Beadle, K., Gradinaru, V., Deverman, B.E., and Anderson, D.J. (2018). The neuropeptide Tac2 controls a distributed brain state induced by chronic social isolation stress. Cell *173*, 1265–1279.e19. https://doi.org/10.1016/j.cell.2018.03.037.
91. Li, H., Namburi, P., Olson, J.M., Borio, M., Lemieux, M.E., Beyeler, A., Calhoon, G.G., Hitora-Imamura, N., Coley, A.A., Libster, A., et al. (2022). Neurotensin orchestrates valence assignment in the amygdala. Nature *608*, 586–592. https://doi.org/10.1038/s41586-022-04964-y.
92. Nam, H., Chandra, R., Francis, T.C., Dias, C., Cheer, J.F., and Lobo, M.K. (2019). Reduced nucleus accumbens enkephalins underlie vulnerability to social defeat stress. Neuropsychopharmacology *44*, 1876–1885. https://doi.org/10.1038/s41386-019-0422-8.
93. Parker, K.E., Pedersen, C.E., Gomez, A.M., Spangler, S.M., Walicki, M.C., Feng, S.Y., Stewart, S.L., Otis, J.M., Al-Hasani, R., McCall, J.G., et al. (2019). A paranigral VTA nociceptin circuit that constrains motivation for reward. Cell *178*, 653–671.e19. https://doi.org/10.1016/j.cell.2019.06.034.
94. Tracy, M.E., Tesic, V., Stamenic, T.T., Joksimovic, S.M., Busquet, N., Jevtovic-Todorovic, V., and Todorovic, S.M. (2018). CaV3.1 isoform of T-type calcium channels supports excitability of rat and mouse ventral tegmental area neurons. Neuropharmacology *135*, 343–354. https://doi.org/10.1016/j.neuropharm.2018.03.028.
95. Wang, H.L., Qi, J., Zhang, S., Wang, H., and Morales, M. (2015). Rewarding effects of optical stimulation of ventral tegmental area glutamatergic neurons. J. Neurosci. *35*, 15948–15954. https://doi.org/10.1523/JNEUROSCI.3428-15.2015.
96. Tan, K.R., Yvon, C., Turiault, M., Mirzabekov, J.J., Doehner, J., Labouèbe, G., Deisseroth, K., Tye, K.M., and Lüscher, C. (2012). GABA

neurons of the VTA drive conditioned place aversion. Neuron *73*, 1173–1183. https://doi.org/10.1016/j.neuron.2012.02.015.

97. van Zessen, R., Phillips, J.L., Budygin, E.A., and Stuber, G.D. (2012). Activation of VTA GABA neurons disrupts reward consumption. Neuron *73*, 1184–1194. https://doi.org/10.1016/j.neuron.2012.02.016.
98. Soden, M.E., Chung, A.S., Cuevas, B., Resnick, J.M., Awatramani, R., and Zweifel, L.S. (2020). Anatomic resolution of neurotransmitter-specific projections to the VTA reveals diversity of GABAergic inputs. Nat. Neurosci. *23*, 968–980. https://doi.org/10.1038/s41593-020-0657-z.
99. Jhou, T.C., Fields, H.L., Baxter, M.G., Saper, C.B., and Holland, P.C. (2009). The rostromedial tegmental nucleus (RMTg), a GABAergic afferent to midbrain dopamine neurons, encodes aversive stimuli and inhibits motor responses. Neuron *61*, 786–800. https://doi.org/10.1016/j.neuron.2009.02.001.
100. Li, H., Pullmann, D., Cho, J.Y., Eid, M., and Jhou, T.C. (2019). Generality and opponency of rostromedial tegmental (RMTg) roles in valence processing. eLife *8*. https://doi.org/10.7554/eLife.41542.
101. Xiao, C., Cho, J.R., Zhou, C., Treweek, J.B., Chan, K., McKinney, S.L., Yang, B., and Gradinaru, V. (2016). Cholinergic mesopontine signals govern locomotion and reward through dissociable midbrain pathways. Neuron *90*, 333–347. https://doi.org/10.1016/j.neuron.2016.03.028.
102. Qi, J., Zhang, S., Wang, H.L., Wang, H., de Jesus Aceves Buendia, J., Hoffman, A.F., Lupica, C.R., Seal, R.P., and Morales, M. (2014). A glutamatergic reward input from the dorsal raphe to ventral tegmental area dopamine neurons. Nat. Commun. *5*, 5390. https://doi.org/10.1038/ncomms6390.
103. Beier, K.T., Steinberg, E.E., DeLoach, K.E., Xie, S., Miyamichi, K., Schwarz, L., Gao, X.J., Kremer, E.J., Malenka, R.C., and Luo, L. (2015). Circuit architecture of VTA dopamine neurons revealed by systematic input-output mapping. Cell *162*, 622–634. https://doi.org/10.1016/j.cell.2015.07.015.
104. Dautan, D., Souza, A.S., Huerta-Ocampo, I., Valencia, M., Assous, M., Witten, I.B., Deisseroth, K., Tepper, J.M., Bolam, J.P., Gerdjikov, T.V., et al. (2016). Segregated cholinergic transmission modulates dopamine neurons integrated in distinct functional circuits. Nat. Neurosci. *19*, 1025–1033. https://doi.org/10.1038/nn.4335.
105. Yoo, J.H., Zell, V., Wu, J., Punta, C., Ramajayam, N., Shen, X., Faget, L., Lilascharoen, V., Lim, B.K., and Hnasko, T.S. (2017). Activation of pedunculopontine glutamate neurons is reinforcing. J. Neurosci. *37*, 38–46. https://doi.org/10.1523/JNEUROSCI.3082-16.2016.
106. Pollak, D.D., Monje, F.J., Zuckerman, L., Denny, C.A., Drew, M.R., and Kandel, E.R. (2008). An animal model of a behavioral intervention for depression. Neuron *60*, 149–161. https://doi.org/10.1016/j.neuron.2008.07.041.
107. Ramirez, S., Liu, X., MacDonald, C.J., Moffa, A., Zhou, J., Redondo, R.L., and Tonegawa, S. (2015). Activating positive memory engrams suppresses depression-like behaviour. Nature *522*, 335–339. https://doi.org/10.1038/nature14514.
108. Zhang, S., Mano, H., Lee, M., Yoshida, W., Kawato, M., Robbins, T.W., and Seymour, B. (2018). The control of tonic pain by active relief learning. eLife *7*. https://doi.org/10.7554/eLife.31949.
109. Zhang, S., Yoshida, W., Mano, H., Yanagisawa, T., Mancini, F., Shibata, K., Kawato, M., and Seymour, B. (2020). Pain control by co-adaptive learning in a brain-machine interface. Curr. Biol. *30*, 3935–3944.e7. https://doi.org/10.1016/j.cub.2020.07.066.
110. Friard, O., and Gamba, M. (2016). BORIS: a free, versatile open-source event-logging software for video/audio coding and live observations. Methods Ecol. Evol. *7*, 1325–1330. https://doi.org/10.1111/2041-210X.12584.
111. Pascoli, V., Terrier, J., Hiver, A., and Lüscher, C. (2015). Sufficiency of mesolimbic dopamine neuron stimulation for the progression to addiction. Neuron *88*, 1054–1066. https://doi.org/10.1016/j.neuron.2015.10.017.
112. Mahn, M., Prigge, M., Ron, S., Levy, R., and Yizhar, O. (2016). Biophysical constraints of optogenetic inhibition at presynaptic terminals. Nat. Neurosci. *19*, 554–556. https://doi.org/10.1038/nn.4266.
113. Zheng, Z., Guo, C., Li, M., Yang, L., Liu, P., Zhang, X., Liu, Y., Guo, X., Cao, S., Dong, Y., et al. (2022). Hypothalamus-habenula potentiation encodes chronic stress experience and drives depression onset. Neuron *110*, 1400–1415.e6. https://doi.org/10.1016/j.neuron.2022.01.011.
114. Li, Y., Zhong, W., Wang, D., Feng, Q., Liu, Z., Zhou, J., Jia, C., Hu, F., Zeng, J., Guo, Q., et al. (2016). Serotonin neurons in the dorsal raphe nucleus encode reward signals. Nat. Commun. *7*, 10503. https://doi.org/10.1038/ncomms10503.
115. Cui, Y., Yang, Y., Ni, Z., Dong, Y., Cai, G., Foncelle, A., Ma, S., Sang, K., Tang, S., Li, Y., et al. (2018). Astroglial Kir4.1 in the lateral habenula drives neuronal bursts in depression. Nature *554*, 323–327. https://doi.org/10.1038/nature25752.
116. Huang, P., Xiang, X., Chen, X., and Li, H. (2020). Somatostatin neurons govern theta oscillations induced by salient visual signals. Cell Rep. *33*, 108415. https://doi.org/10.1016/j.celrep.2020.108415.
117. Kvitsiani, D., Ranade, S., Hangya, B., Taniguchi, H., Huang, J.Z., and Kepecs, A. (2013). Distinct behavioural and network correlates of two interneuron types in prefrontal cortex. Nature *498*, 363–366. https://doi.org/10.1038/nature12176.

Please cite this article in press as: Dong et al., Stress relief as a natural resilience mechanism against depression-like behaviors, Neuron (2023), https://doi.org/10.1016/j.neuron.2023.09.004

STAR★METHODS

KEY RESOURCES TABLE

REAGENT or RESOURCE	SOURCE	IDENTIFIER
Antibodies		
Rabbit anti-tyrosine hydroxylase	Santa Cruz	Cat# SC-14007
Goat anti-rabbit Alexa Fluor 546	Invitrogen	Cat# A-11035; RRID: AB_143051
Bacterial and virus strains		
AAV2/9-CAG-DIO-GCaMP6s	Taitool Bioscience Ltd., Shanghai	Cat# S0354-9-H50
AAV2/9-EF1α-DIO-eNpHR3.0-mCherry	OBiO Technology Ltd., Shanghai	Cat# H4882
AAV2/9-EF1α-DIO-hChR2(H134R)-mCherry	OBiO Technology Ltd., Shanghai	Cat# AG20297
AAV2/9-EF1α-DIO-EYFP	OBiO Technology Ltd., Shanghai	Cat# AG20296
AAV2/9-hSyn-DA2m	WZ Biosciences Inc., Shandong	Cat# YL002009-AV9-PUB
Chemicals, peptides, and recombinant proteins		
DAPI	Solarbio	Cat# S2110
Hoechst	Selleck	Cat# S0485
Pentobarbital sodium	Sigma	Cat# P3761
Morphine	Shenyang Pharmaceutical.	Cat# XN02AAM022B002010201161
SCH23390	Sigma	Cat# D054
Milk chocolate	Dove	N/A
Experimental models: Organisms/strains		
Mouse: C57BL/6J	SLAC Laboratory animal, Shanghai	N/A
Mouse: DAT-Cre	Jackson Laboratory	RRID:IMSR_JAX:020080
Mouse: D1R-Cre	Mutant Mouse Resource Research Centers	RRID:MMRRC_030989-UCD
Software and algorithms		
GraphPad Prism 8	GraphPad software	https://www.graphpad.com/
MATLAB_R2020a	MathWorks	https://www.mathworks.com/
Any-Maze	Stoelting	https://www.any-maze.com/
Inper Studio (optogenetics and fiber photometry)	Inper, China	https://www.inper.com/
Inper Data Process (fiber photometry)	Inper, China	https://www.inper.com/
CamFibrePhotometry (fiber photometry)	ThinkerTech, Nanjing	http://www.thinkerbiotech.com/
BORIS	Friard and Gamba[110]	http://www.boris.unito.it/
ImageJ	National Institutes of Health	https://imagej.nih.gov/ij/index.html
OmniPlex neural recording data acquisition system	Plexon	https://plexon.com/products/omniplex-software
NeuroExplorer	Plexon	https://plexon.com/products/neuroexplorer
Offline sorter	Plexon	https://plexon.com/products/offline-sorter
Software and algorithms		
473-nm and 589-nm laser LED	Inper, China	https://www.inper.com/
Fiber photometry	ThinkerTech, Nanjing; Inper, China	http://www.thinkerbiotech.com/ https://www.inper.com/

RESOURCE AVAILABILITY

Lead contact

Further information and requests for resources and reagents may be directed to and will be fulfilled by the lead contact, Hailan Hu (huhailan@zju.edu.cn).

Materials availability

This study did not generate new unique reagents.

Data and code availability

- All data reported in this paper will be shared by the lead contact upon request.
- This paper does not report original code.
- Any additional information required to reanalyze the data reported in this paper is available from the lead contact upon request.

EXPERIMENTAL MODEL AND STUDY PARTICIPANT DETAILS

Animals

Male adult (8-12 weeks of age) C57/BL6j mice (SLAC Laboratory Animal Co., Shanghai; Jihui Laboratory Animal Co., Shanghai), DAT-Cre mice (8-24 weeks of age, Jackson Laboratory, stock number: 020080) and D1R-Cre mice (8-16 weeks of age, Mutant Mouse Resource Research Centers, stock number: 030989) were used. Mice were housed two to five per cage under a 12-h light–dark cycle (light on from 7 a.m. to 7 p.m.) with free access to food and water ad libitum. Mice were habituated in the behavioral rooms for 0.5-1h before all the behavioral tests. All animal studies and experimental procedures were approved by the Animal Care and Use Committee of the animal facility at Zhejiang University.

METHOD DETAILS

Drugs and treatments

The following drugs were dissolved in 0.9% saline, and administered intraperitoneally (i.p.). Concentrations were as follows: pentobarbital sodium (100 mg/kg, Sigma), morphine (10 mg/kg, Shenyang Pharmaceutical.) and SCH23390 (0.1 mg/kg, Sigma). In Res-Rew experiments, milk chocolate (Dove) in size similar to food pellet and 2% sucrose were provided in homecage during the 14-day CRS.

Stereotaxic surgeries

Mice were deeply anaesthetized by pentobarbital sodium, and then placed in a stereotactic frame (RWD Instruments). Virus (200 nL) was injected unilaterally or bilaterally in VTA (AP, − 3.0 ∼ − 3.2 mm from bregma; ML, ± 0.5 mm; DV, − 4.3 mm from the dura), NAcLat (AP, + 1.2 mm from bregma; ML, ± 2.0 mm; DV, − 4.0 mm from the dura), or dNAcMed (AP, + 1.5 mm from bregma; ML, ± 0.65 mm; DV, − 3.9 mm from the dura) using a pulled glass capillary with a pressure microinjector (Picospritzer III, Parker) at a rate of 100 nL/min. The injection needle was withdrawn 10 min after ending injection. After surgery, mice were allowed to recover from anaesthesia on a heat pad. For optic fiber implantation in the calcium photometry of VTA-DA somata, a 200-μm optic fiber cannula (NA = 0.37, Inper Ltd., China) was placed 200-250 μm above the viral injection site, and cemented onto the skull using dental cement. Given the distinct functions of DA projections to the dNAcMed and NAc ventromedial shell (vNAcMed),[23,70] for dNAcMed DA terminal manipulations, optic fibers were bilaterally implanted at a 20° angle (AP, + 1.5 mm from bregma; ML, ± 1.9 mm; DV, − 3.2 mm from the dura) to avoid interventing the vNAcMed. For optogenetic manipulations of NAcLat DA terminals, optic fibers were implanted to the NAcLat (AP, + 1.2 mm from bregma; ML, ± 2.0 mm; DV, − 3.6 mm from the dura). For fiber photometry of DA terminal calcium signals or DA release in the NAc, optic fibers were implanted to NAcLat (AP, + 1.2 mm from bregma; ML, ± 2.0 mm; DV, − 3.8 mm from the dura), dNAcMed (AP, + 1.5 mm from bregma; ML, ± 0.65 mm; DV, − 3.7 mm from the dura). AAVs used in this study were from OBiO Technology Ltd., Shanghai (AAV2/9-EF1α-DIO-eNpHR3.0-mCherry; AAV2/9-EF1α-DIO-hChR2(H134R)-mCherry; AAV2/9-EF1α-DIO-EYFP; diluted to ∼ 10^{12} vector genome (v.g.) /mL), WZ Biosciences Inc., Shandong (AAV2/9-hSyn-DA2m, diluted to ∼ 10^{13} v.g./mL) and Taitool Bioscience Ltd., Shanghai (AAV2/9-CAG-DIO-GCaMP6s, diluted to ∼ 10^{12} v.g./mL). All mice used in behavioural assays were allowed to recover from surgery for 2 ∼ 4 weeks before soma fiber photometry, 6 weeks before terminal fiber photometry and terminal optogenetic manipulations.

Optogenetic stimulation assays

Optic fiber implants were connected to a patch cable with a ceramic sleeve (Inper Ltd., China), which was connected to a commutator (Doric, Canada) via an FC/PC adapter to allow unrestricted movement. A second patch cable, with a FC/PC connector at either end (Inper Ltd., China), was connected to the commutator and then connected to a diode-pumped solid state (DPSS) 473-nm or 589-nm laser (Inper Ltd., China). For terminal activation, 473-nm blue laser (10-12 mW from the optic fiber tip) was delivered at 20 Hz, 10-ms pulse width, 5 pulses per 0.5 second to mimic physiological DA firings when mice received reward.[111] For terminal inhibition, 589-nm yellow light was delivered constantly (10-15 mW from the optic fiber tip) and terminated by a 10-second ramping down protocol to attenuate the rebound effect of eNpHR3.0.[21,64,112] The duration of optogenetic stimulation was determined according to the DA terminal calcium activity and DA release in the dNAcMed (which has about 10-min persistent activation) and NAcLat (which shows 6 ∼ 20-second transient activation and has significantly more sporadic calcium transients than in homecage baseline for 4∼5min after stress termination).

Please cite this article in press as: Dong et al., Stress relief as a natural resilience mechanism against depression-like behaviors, Neuron (2023), https://doi.org/10.1016/j.neuron.2023.09.004

Behavioral assays

Conditioned place preference (CPP)

CPP was performed in a custom-made two-chamber apparatus (50 cm × 25 cm × 30 cm), with a buffer room (20 cm × 15 cm × 30 cm) to the side of two chambers. CPP consisted of three phases:

(1) Pre-test phase on day 1 and 2. Mice were gently placed into the buffer room, allowed to freely choose either chamber and then freely explore the two chambers for 15 min. Once the mice entered one of the two chambers, the door between the buffer room and the two chambers were closed. The time spent in the less preferred chamber on day 2 was used as the baseline.

(2) Conditioning on day 3 and 4. For relief CPP, mice were firstly confined in the preferred chamber for 30 min in the morning (blank pairing). 4-5 hours later, mice were subjected to 30-min restraint (Res) or footshock (FS) stress, or subjected to blank pairing again for the blank group. As soon as the stressor was terminated, mice were instantly confined in the less preferred chamber for 30 min (relief pairing). For the 30-min restraint stress, two sizes of tubes were used: wide tubes (transparent Plexiglas tubes with holes for air flow, 3.2-cm inside diameter, 12-cm length), and narrow tubes (50-mL conical tubes with holes for air flow, 2.5-cm inside diameter, 10-cm length). 30-min restraint in such narrow tubes was employed if not particularly described. For the D1R systemic blockade experiments, SCH23390 was injected (i.p.) immediately following the termination of restraint stress. For the FS stress, 10 shocks (0.5 mA, 2-s duration) were randomly delivered to mice within 5 min in a fear conditioning chamber (Coulbourn Instruments, U.S.). For the time window characterization of Res-relief, mice were confined in the less preferred chamber with or without the time delay (0, 5, 10, 15, 30 or 60 min) after terminating the restraint stress. For optogenetic inhibition experiments of CPP, transparent Plexiglas narrow tubes (2.5-cm inside diameter, 10-cm length) were used for 30-min restraint, with holes for air flow and grooved for optic fibers passing through. 5-min (for eNpHR3.0 in inhibiting NAcLat DA terminals) or 10-min (for eNpHR3.0 in inhibiting dNAcMed DA terminals) 589-nm laser was delivered 1-3 seconds before picking up restraint tubes to release mice. For the morphine CPP, mice were firstly injected with saline (i.p.) and confined in the preferred chamber for 30 min. 4-5 hours later, mice were injected with morphine (i.p., 10 mg/kg) and confined in the less preferred chamber for 30 min.

(3) Test on day 5. The same procedure as the pre-test, mice were allowed to freely explore the two chambers for 15 min. A video camera positioned directly above the arena was used to track each mouse via Any-maze software (Stoelting, U.S.). CPP score was calculated as $(\text{Time in relief- or morphine-paired chamber})_{\text{test}} - (\text{Time in the same chamber})_{\text{pre-test}}$. Heat maps were made by MATLAB (MathWorks).

Chronic restraint stress (CRS)

In normal CRS protocol, mice were placed in narrow restraint tubes for 2-3 hours per day for 14 consecutive days.[42] For optogenetic activation, 5-min (for ChR2 in activating NAcLat DA terminals) and 10-min (for ChR2 in activating dNAcMed DA terminals) 473-nm laser was delivered instantly after daily restraint. In subthreshold CRS protocol, mice were subjected to restraint stress (narrow tubes) for 3 days.[113] For optogenetic inhibition, 5-min (for eNpHR3.0 in inhibiting NAcLat DA terminals) or 10-min (for eNpHR3.0 in inhibiting dNAcMed DA terminals) 589-nm laser was delivered 1-3 seconds before picking up restraint tubes to release mice. For D1R systemic blockade, SCH23390 was i.p. injected instantly or with a 10-min or 2-hour delay after daily restraint. For Res-Rew experiments, chocolate and 2 % sucrose were provided *ad libitum* instantly or with 2-hour delay after daily restraint. For 2-hour natural reward experiments, chocolate and 2% sucrose were provided only for 2 hours instantly or with 2-hour delay after daily restraint.

Open field test

In a room with dim light (5-10 lux), mice were gently placed in the centre of an arena (40 cm × 40 cm × 40.5 cm) and allowed to freely explore for 10 min. A video camera positioned directly above the arena was used to track the movement of each mouse via Any-maze software (Stoelting, U.S.). Total distance was used to evaluate the locomotion ability, and time in center zone was used to evaluate the anxiety level.

Elevated plus maze test

Mice were handled 1-2 min/day for 3 days before testing. Mice were gently placed in the center of maze, with the head orienting to the open arm. Mice were allowed freely explore the elevated plus maze for 5 min. A video camera positioned directly above the arena was used to track each mouse via Any-maze software (Stoelting, U.S.). Time spent in open arm was used to evaluate the anxiety level.

Novelty-suppressed feeding test

After food deprivation for 24 hours in homecage, mice were gently placed in the corner of an open field apparatus with normal new beddings and a single food pellet at the center on a 1 cm^2 elevated platform. Illumination intensity in the center zone (~ 100 lux) is higher than the peripheral zone (~ 50 lux). Mice were allowed to freely explore for 10 min. The latency to feeding was defined as the time spent for mice getting the first bite of food pellet. After the 10-min test, mice were placed back into their homecage and given another single food pellet, which was weighted before and after a 5-min consumption to measure the effects of motivation and hunger on feeding behaviors.

Forced swim test

Mice were individually placed in a cylinder (12 cm diameter, 25 cm height) of water (23-24 °C) and swam for 6 min under normal illumination (100-200 lux). Water depth was set to prevent mice from touching the bottom with their tails or hind limbs. Mouse behaviours were videotaped from the side. The immobile duration during the last 4-min test and the latency to the 1st immobility lasting for more than 3 s were counted offline by an experienced observer blinded to the animal treatments. Immobile duration was defined as the time spent in floating, or only having movements necessary for keeping balance in the water without shaking the body trunk or the center of gravity. For mice with optogenetic manipulations, the patch cable length was tensioned and adjusted to 5-10 mm above the center of water surface, in order to minimize the impact of patch cable on swimming behaviour, and prevent water entering the crevice around the dental cement and avoid mice drowning.

Sucrose preference test

Mice were single housed and habituated with two bottles of water for 2 days, followed by two bottles of 2% sucrose in 2-hour acute SPT or 1% sucrose in 48-hour chronic SPT for 2 days. During the 4-day habituation period, bottle positions were switched every morning, and bottles were weighted every morning and every night to calculate baseline preference. Notably, the bottles were replaced if their baseline preference (averaged preference of the day and the night periods) higher than 80% or lower than 20%, in order to eliminate the interference of baseline preference on the following test. For acute SPT, after the habituation period, mice were water deprived for 24 hours and then exposed to one bottle of 2% sucrose and the other bottle of water for 2 hours in the active phase of mice (to increase the liquid consumption). Bottle positions were switched every half an hour and bottles were weighted every 1 hour. For chronic SPT, after the habituation period, mice were exposed to one bottle of 1% sucrose and the other bottle of water for 48 hours. Bottle positions were switched and bottles were weighted every 24 hours. Sucrose preference was defined as the average sucrose consumption percentage during the 1st and 2nd hours (in acute SPT), or during the 1st and 2nd 24 hours (in chronic SPT). Acute SPT was performed after 14-day CRS protocol, and chronic SPT was performed after 3-day subthreshold CRS protocol.

Real time place preference

Mice were gently placed in a white chamber (52 cm × 26 cm × 23 cm) consisting of two identical chambers, and allowed to freely explore chambers for 20 min. Stimulated side was assigned in a counterbalanced manner. 473-nm laser stimulation (20 Hz, 10-ms pulse width, 5 pulses per 0.5 second) was delivered as soon as mice entered the stimulated side and terminated once mice crossed to the non-stimulated side. A video camera positioned above the chamber tracked each mouse by Any-maze software (Stoelting, U.S.). Time percent spent in the light ON side is calculated as (Time in stimulated side) ÷ 1200 × 100 %.

Fiber photometry

GCaMP6s and DA2m fluorescence signals were obtained with the fiber photometry apparatus (Thinker Tech Nanjing Biotech Ltd., or Inper Ltd.) and sampled at the frequency of 50 or 100 frames per second. Intensity of 470-nm LED was controled 20 ∼ 40 μW at the optic fiber tip. During recording, a video camera was positioned above the chamber to track each mouse. Mouse behaviors and fluorescence signals were simultaneously captured in the same screen recording, in order to align the time point of behavioral events with the fluorescence signals of calcium activity and dopamine release. Before recording, mice were habituated in the recording room for 1 hour. Mice were then gently connected to patch cables and placed back to homecage. Other cagemates were transferred to another cage until the next recording session.

In Res-relief design, the 1st day recording session aimed to habituate mice and measure the signals of control condition which minimized the relief signals.The 1st day recording session consisted of 4 steps: (1) Habituation to patch cables in homecage. During this period, mice were allowed freely move in homecage for 10 min. (2) Habituation to novel context of relief chamber. During this period, mice were gently placed in relief chamber and allowed to freely explore for 10 min. (3) Habituation to the restraint tube. During this period, the gate of relief chamber was open and connected with the restraint tube. Mice were put into the restraint tube and allowed to freely go through the tube to enter the relief chamber. This process was repeated for at least 6 times. If mice intensely struggled and screamed when put into the restraint tube, more times of this process were repeated to minimize the relief signals, because strong resistance of mice indicated strong aversion and probably evoked relief afterwards. (4) Record the signals of control condition. During this period, the gate was closed first and mice were put into the restraint tube. As soon as mice entered the restraint tube, the gate was open and mice were allowed to voluntarily enter the relief chamber. After that, the gate was instantly closed again. Mice were then allowed to freely explore the relief chamber for at least 2 min. This process was repeated for 6 times. Restraint tube was cleaned after recording each mouse.

Recording sessions starting from the 2nd day were conducted to measure the relief signals. Only one Res-relief recording session was conducted within a single day and consisted of 3 steps: (1) Record the baseline signals in homecage. In this period, mice were allowed freely move in homecage for 10 min. (2) Record the signals during restraint. During 30-min restraint stress, 470-nm LED was turned off unless recording the first and the last 2 min, in order to reduce the photobleaching effects. (3) Record the relief signals. After completing 30-min restraint, the gate was rapidly open and mice were allowed to voluntarily enter the relief chamber. After that, the gate was instantly closed. Mice were then allowed to freely explore the relief chamber for 10 ∼ 30 min.

Mouse behaviors were manually annotated via BORIS software.[110] MATLAB codes (from Thinker Tech Nanjing Biotech Co., Ltd) were used to analyze fluorescence signals. As previously described,[114] permutation test was applied to determine the time periods

when fluorescence signals during relief were significantly increased compared to the baseline condition. Baseline signals for making permutations were obtained as the 120-s period before relief onset or within homecage. We used 1,000 permutations for an α-level set as 0.05 to compare the fluorescence values of relief and baseline. Statistical significance at each time point was generated, and signal curves were annotated in red if $p < 0.05$. For comparison of signal curves between relief and control groups, fluorescence signals of 5-second period before gate open were used as the baseline condition. According to fluorescence kinetics under different recording conditions, peak amplitude in individual trials was obtained within 5 seconds after relief onset. Area under curve (AUC) was calculated as the sum of fluorescence signals during the relevant periods.

In vitro electrophysiology

VTA brain slice preparation was performed as previously described.[113,115] In brief, DAT-Cre mice expressing Cre-dependent ChR2 (11-16 weeks of age) were anaesthetized with 10% chloral hydrate, and then perfused with 20 ml ice-cold artificial cerebrospinal fluid (ACSF) (oxygenated with 95% O2 + 5% CO2) containing (mM): 125 NaCl, 2.5 KCl, 25 $NaHCO_3$, 1.25 NaH_2PO_4, 1 $MgCl_2$, 2 $CaCl_2$, 25 glucose and 1 pyruvate. The brain was dissected as soon as possible after decapitation and put into chilled and oxygenated ACSF. Coronal slices containing the VTA (300 μm thickness) were sectioned in cold ACSF using a Leica2000 vibratome and then transferred to ACSF at 32 °C for incubation and recovery. ACSF was continuously gassed with 95% O2 and 5% CO2. Slices were allowed to recover for at least 1 h before recording. Whole-cell patch-clamp recordings were performed in VTA-DA neurons, using pipettes with a typical resistance of 5–6 MΩ filled with internal solution containing (mM): 105 K-gluconate, 30 KCl, 4 Mg-ATP, 0.3 Na-GTP, 0.3 EGTA, 10 HEPES and 10 Na-phosphocreatine, with pH set to 7.35. The external ACSF contained (mM): 125 NaCl, 2.5 KCl, 25 $NaHCO_3$, 1.25 NaH_2PO_4, 1 $MgCl_2$, 2 $CaCl_2$ and 25 glucose. Neurons were visualized with infrared light and mCherry fluorescence was confirmed with 550-nm light on an upright microscope (BX51WI, Olympus). A MultiClamp 700B amplifier and pCLAMP10 software (Molecular Devices) were used for slice recordings (Axon Instruments). The series resistance and capacitance were compensated automatically after a stable Gigaseal was formed. Recorded neurons were discarded if a change in series resistance was above 20%. The resting membrane potential (RMP) and action potentials of a neuron were obtained under current clamp (I = 0 pA). For verifying the efficiency of ChR2 activation, 10-mW 473-nm laser was delivered at 20 Hz, 5 pulses per 0.5 second.

In vivo optrode recording in freely moving mice

As previously described,[116,117] a custom-made microdrive guide tube housed 16 electrodes (35.6 μm diameter, impedance 250–500 KΩ, California Fine Wire Co.) and an optic fiber was implanted into the VTA (AP, − 3.0 ∼ − 3.2 mm from bregma; ML, + 0.5 mm; DV, − 4.0 mm from the dura) of DAT-Cre mice after 3-week expression of Cre-dependent ChR2 virus. The tip of optic fiber was 200-400 μm above the tip of electrodes. Stainless steel wires were attached to two screws on the skull as ground. The microdrive was secured to the skull with dental cement. After recovery for 1 week, mice were allowed to adapt to the recording headstage for 10 min per day for 2-3 days. Spontaneous spiking activity (digitized at 40 kHz, band-pass filtered between 300 and 6,000 Hz) was recorded in homecage with a gain of 5,000×. The optrodes were lowered in steps of 50 μm after each recording session, followed by at least 1-day recovery. All waveforms recorded from each electrode were imported in Offline Sorter V4 (Plexon Inc.). Single units were manually identified by threshold crossing and principal component analysis (PCA). Spikes with inter-spike interval (ISI) less than the refractory period (1.4 ms) were excluded. Only high-quality units (L ratio < 0.01, isolation distance > 20) were included.

For *in vivo* DA opto-tagging experiments, 2-minute photostimulation (473-nm laser, 1 Hz, 10-ms pulse width, 10 mW) was performed before and after each recording session. Each recording session contained 10-minute homecage baseline, and 5 trials each consisting of restraint and relief. The duration of restraint and relief were both shortened to 10 minutes, due to the time limit of continuous recording within the same day. Neurons were classified as tagged DA neurons if light-evoked spikes had high responsive fidelity (> 80%), short latency (< 10 ms) and highly correlated waveforms with spontaneous spikes (Pearson's correlation coefficient > 0.9). All data analyses were performed using MATLAB_R2020a as previously described.[116] To classify putative DA neurons, electrophysiological criteria were used based on the valley full-width half maximum (FWHM) and spontaneous firing rate.[46] Putative DA neurons were identified if the valley FWHM was wider than 500 μs and the spontaneous firing rate was lower than 10 Hz. For Res-relief recording, DA neuronal activity was aligned to the relief onset. Z score was applied to normalize the firing rate (bin = 5 s), by subtracting the average firing rate of homecage baseline and dividing the standard deviation of homecage baseline. Z score < -2 or > 2 statistically corresponds to $p < 0.05$, so Z score < -2 is used as the threshold of inhibition and Z score > 2 is used as the threshold of activation.

Histological verifications and immunohistochemistry

Mice were anaesthetized with 0.2 mL 10% chloral hydrate, and then intracardially perfused with 20 mL PBS and 20 mL 4% paraformaldehyde in PBS. After decapitation, the whole head of mice with optic fiber or optrode implants were post-fixed in 4% paraformaldehyde in PBS under room temperature for 24 hours (for optic fibers) or 48 hours (for optrodes), in order to make clear of the track of optic fibers or optrodes. Brains were then dissected and post-fixed in 4% paraformaldehyde in PBS under room temperature for 12 hours, followed by cryoprotection in 30% sucrose solution for 24 hours. Coronal slices (50 μm) were sectioned on a cryostat microtome (Leica) and collected in PBS and stored at 4 °C for further use. Slices for verifying virus expression profiles and optic fiber locations were co-stained with Hoechst or DAPI. For tyrosine hydroxylase (TH) staining, slices were stained for 24 hours in primary antibodies (rabbit anti-TH, 1:1000, Santa Cruz). After that, slices were stained for 2 hours in secondary antibodies (Alexa Fluor

Please cite this article in press as: Dong et al., Stress relief as a natural resilience mechanism against depression-like behaviors, Neuron (2023), https://doi.org/10.1016/j.neuron.2023.09.004

546 goat anti-rabbit IgG, 1:1000, Invitrogen). Fluorescent images were acquired by an Olympus MVX10 Macro Zoom microscope, an Olympus VS120 microscope or a Nikon A1 confocal microscope.

QUANTIFICATION AND STATISTICAL ANALYSIS

Required sample sizes were estimated on the basis of our past experience performing similar experiments. Mice were randomly assigned to treatment groups. Statistical analyses were performed using GraphPad Prism V8. By pre-established criteria, values were excluded from analyses if virus expression was poor or optic fiber location was out of the interested region. All statistical tests were two-tailed, and significance was assigned at $p < 0.05$. Normality and equal variances between group samples were assessed using the D'Agostino & Pearson normality test (or Shapiro-Wilk normality test if $n < 8$) and Brown–Forsythe tests, respectively. When normality and equal variance between sample groups was achieved, ordinary one-way ANOVA (followed by Bonferroni's multiple comparisons test or Holm-Sidak's multiple comparisons test), unpaired or paired *t*-test were used. When normality of samples was achieved but equal variance failed, unpaired *t*-test with Welch's correction, or Brown-Forsythe ANOVA test (followed by Dunnett's T3 multiple comparisons test) was performed. When normality failed, Kruskal-Wallis test (followed by Dunn's multiple comparisons test), or Mann-Whitney test was performed. Pearson's or Spearman correlation analysis was performed when normality of samples was achieved or not, respectively. Detailed statistical information is reported in Table S1.

Neuron, Volume *111*

Supplemental information

Stress relief as a natural resilience mechanism against depression-like behaviors

Yiyan Dong, Yifei Li, Xinkuan Xiang, Zhuo-Cheng Xiao, Ji Hu, Yulong Li, Haohong Li, and Hailan Hu

Supplementary Figures and legends:

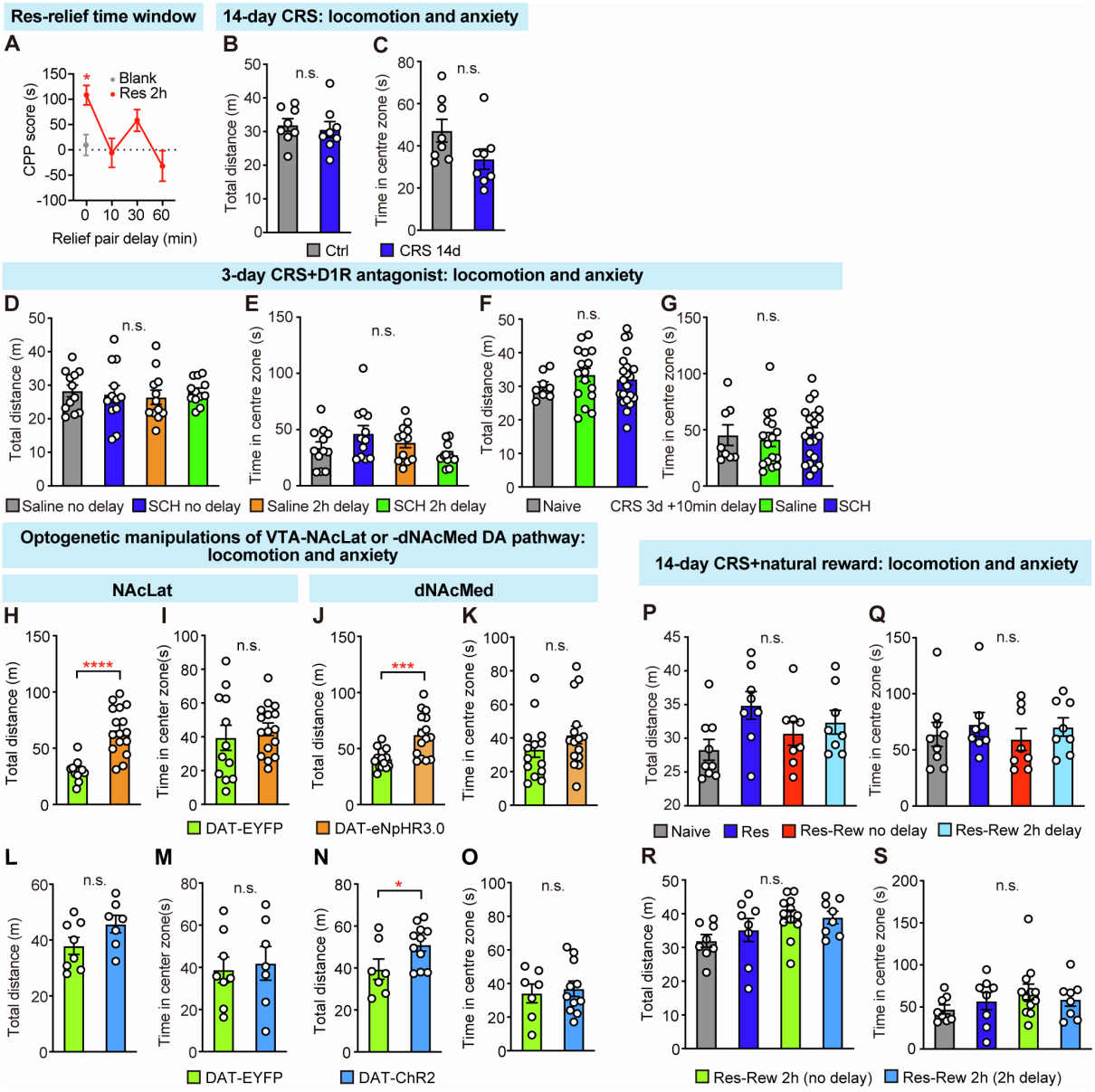

Figure S1. Time window of Res 2h-relief and OFT in all experiments, related to Figures 2, 5, 6 and 7

(A) Time window of relief CPP induced by the termination of 2-hour restraint.

(B-G) Locomotion and anxiety level in OFT of 14-day CRS (B, C), subthreshold 3-day CRS with systemic D1R blockade (with or without 2-hour delay) (D, E), and subthreshold 3-day CRS with systemic D1R blockade (with 10-min delay) (F, G) experiments.

(H and I) Locomotion (H) and anxiety level (I) in OFT after subthreshold 3-day CRS with NAcLat DA terminal photoinhibition.

(J and K) Locomotion (J) and anxiety level (K) in OFT after subthreshold 3-day CRS with dNAcMed DA terminal photoinhibition.

(L and M) Locomotion (L) and anxiety level (M) in OFT after 14-day CRS with NAcLat DA terminal photostimulation.

(N and O) Locomotion (N) and anxiety level (O) in OFT after 14-day CRS with dNAcMed DA terminal photostimulation.
(P-S) Locomotion and anxiety level in OFT of Res-Rew *ad libitum* (P, Q) and Res-Rew 2h experiments (R, S).
n.s., not significant; *p <0.05; ***p <0.001; ****p <0.0001; data represent means ± SEM. See also Table S1.

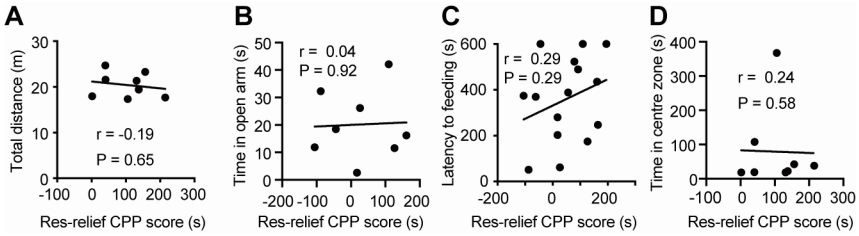

Figure S2. Correlations between stress relief and locomotion or anxiety, related to Figure 2

(A) Correlation between Res-relief CPP score and locomotion in OFT.

(B-D) Correlations between Res-relief CPP score and anxiety level in EPMT (B), NSFT (C) and OFT (D).

See also Table S1.

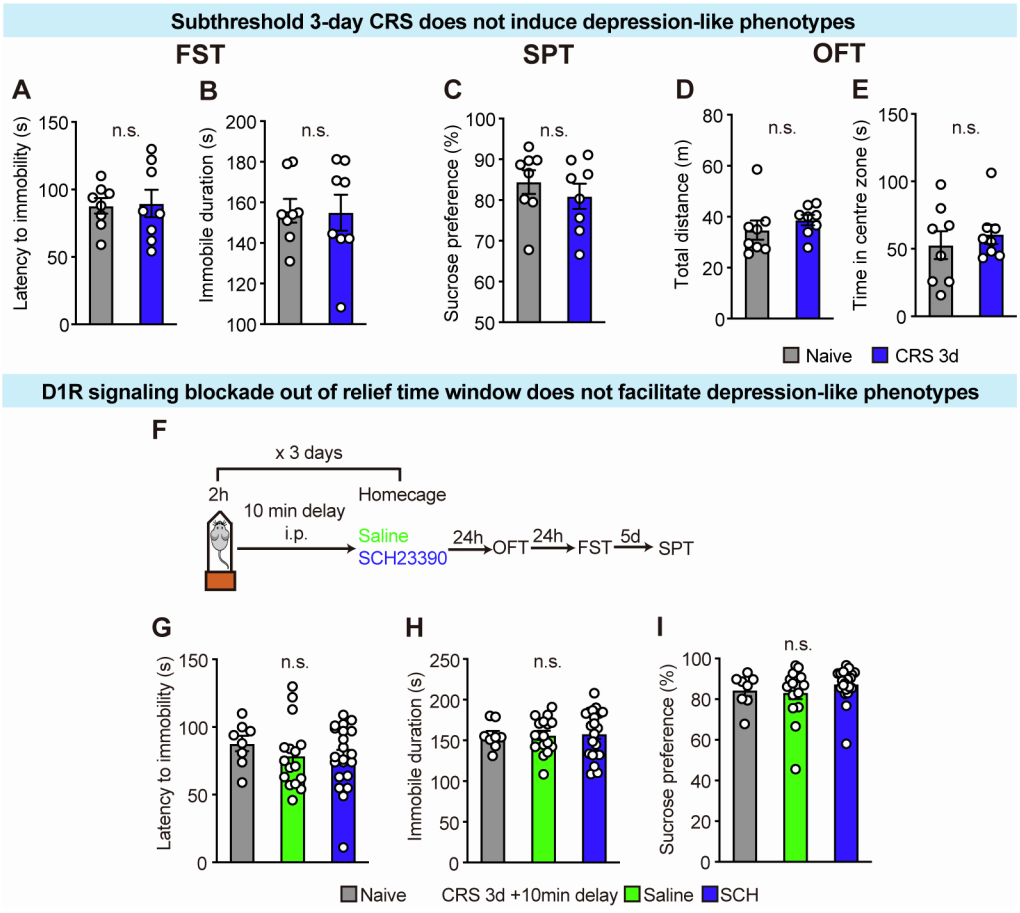

Figure S3. Behavioral results of sub-threshold 3-day CRS model and D1R blockade out of relief period, related to Figure 2

(A-C) Depression-like phenotypes of naïve and subthreshold 3-day CRS groups in latency to immobility (A), immobile duration (B) and sucrose preference (C).

(D and E) locomotion (D) and anxiety level (E) in OFT of naïve and subthreshold 3-day CRS groups.

(F-I) Behavioral paradigm of systemic D1R blockade with 10-min delay after terminating daily restraint during subthreshold 3-day CRS (F), and subsequent depression-like phenotypes developed in FST (G, H) and SPT (I).

n.s., not significant; data represent means ± SEM. See also Table S1.

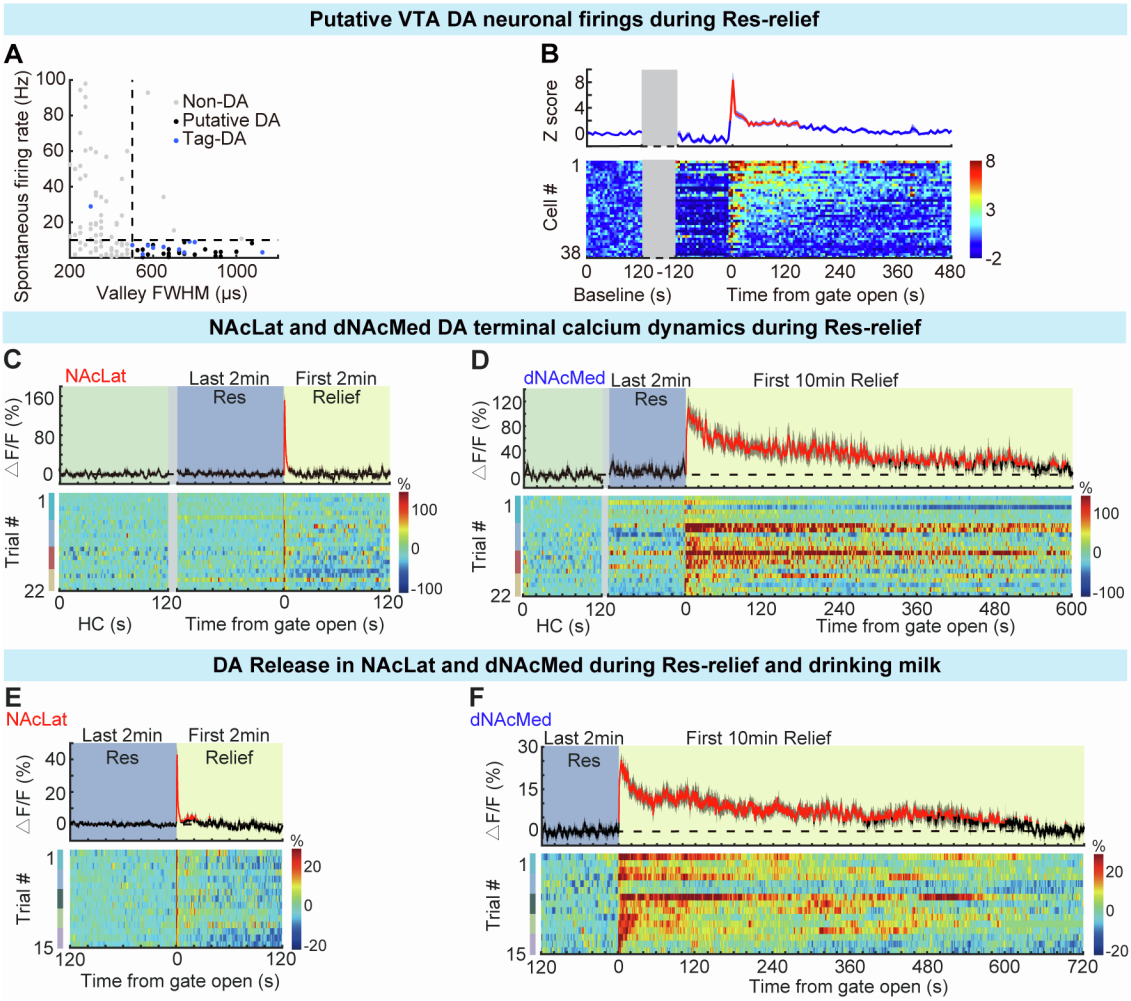

Figure S4. VTA putative DA neuronal firing, terminal calcium activity and DA release in NAc, related to Figures 3 and 4

(A) Classification of recorded VTA neurons based on FWHM of waveform valley and spontaneous firing rate.

(B) Firing Z score of VTA putative DA neurons aligned to the time point of gate open (top) and corresponding heat maps (bottom) ordered by the activation magnitude during relief period.

(C and D) Calcium signals of NAcLat (C) or dNAcMed (D) DA terminals aligned to the time point of gate open (top) and corresponding heat maps (bottom).

(E and F) DA signals in NAcLat (E) or dNAcMed (F) aligned to the time point of gate open (top) and corresponding heat maps (bottom).

Firing Z score, calcium or DA signals significantly higher than baseline are annotated in red. In corresponding heat maps, mouse individuals are annotated by different color bars at the left. See also Table S1.

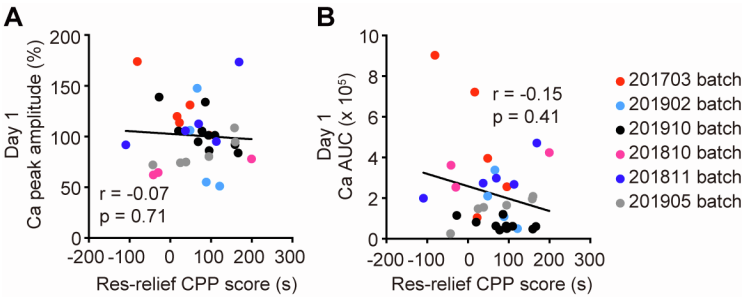

Figure S5. Correlations between Res-relief CPP score and DA soma calcium signals, related to Figure 3

(A and B) Correlations between Res-relief CPP score and VTA-DA soma calcium signals during the 1st day relief pairing: calcium peak amplitude (A) and AUC (B) of VTA-DA soma (6 batches in total).

See also Table S1.

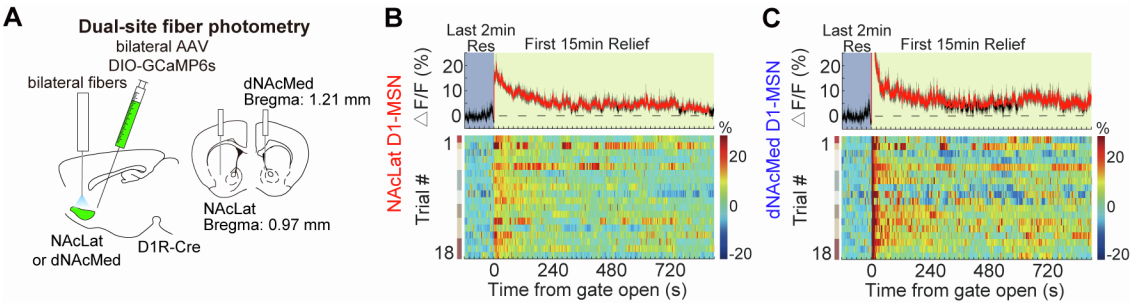

Figure S6. Stress relief persistently activates D1-MSNs in both NAcLat and dNAcMed, related to Figure 4

(A) Schematics of simultaneous dual-site fiber photometry of D1-MSN calcium signals in NAcLat and dNAcMed.

(B and C) Calcium signals of NAcLat (B) and dNAcMed (C) D1-MSNs aligned to the time point of gate open (top) and corresponding heat maps (bottom).

See also Table S1.

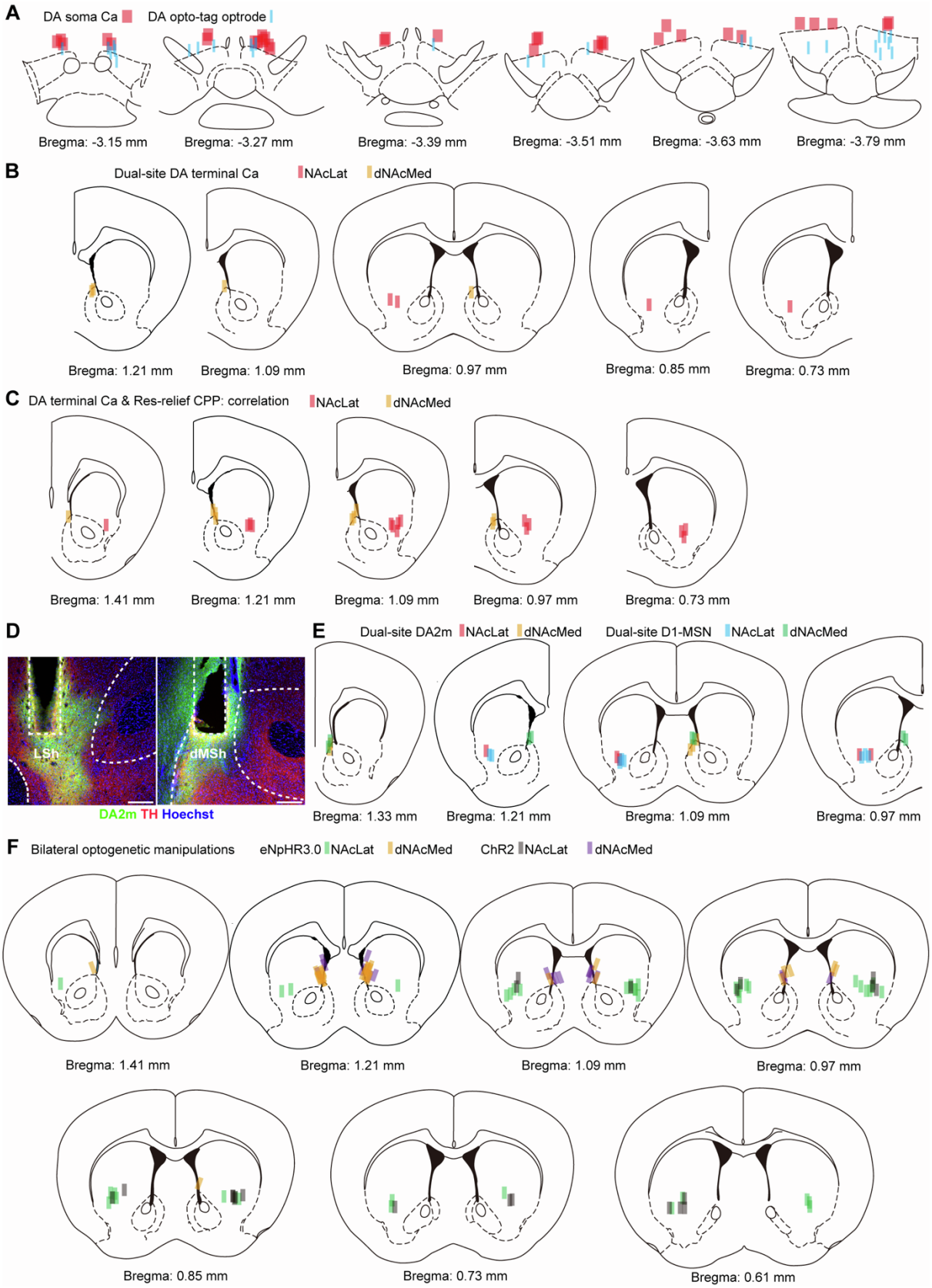

Figure S7. Histological verifications of optic fibers and optrodes, related to Figures 3-6

(A) Verifications of optic fiber locations in VTA-DA soma calcium recordings and optrode locations in VTA-DA opto-tagging recordings.
(B) Verifications of optic fiber locations in NAcLat and dNAcMed dual-site DA terminal calcium photometry.
(C) Verifications of optic fiber locations in measuring correlations between Res-relief CPP score and calcium signals of NAcLat or dNAcMed DA terminals.
(D) Verifications of DA sensor (DA2m) expression profile in NAcLat and dNAcMed. Scale bar, 200 μm.
(E) Optic fiber locations in NAcLat and dNAcMed of DA2m and D1-MSN photometry experiments.
(F) Verifications of optic fiber locations in NAcLat or dNAcMed DA terminal optogenetic manipulations.